Final Report

for

AFOSR grant F49620-96-1-0331

AASERT97

Film Cooling Visualization and Heat Transfer on Transonic Turbine Blades

AFOSR Program Manager
Dr. Tom J. Beutner
AFOSR/NA
801 N. Randolph St., Rm 732
Arlington, VA 22203-1977

Prepared by

Professor Thomas E. Diller
Department of Mechanical Engineering
Virginia Tech
Blacksburg, VA 24061-0237

March 2001

REPORT DOCUMENTATION PAGE

AFRL-SR-BL-TR-01-

0223

1. AGENCY USE ONLY *(Leave blank)*	2. REPORT DATE	3. REPORT T
	MARCH 2001	FINAL TECHNICAL REPORT 1 Jun 97 – 30 Sep 00

4. TITLE AND SUBTITLE
FILM COOLING VISUALIZATION AND HEAT TRANSFER ON TRANSONIC TURBINE BLADES

5. FUNDING NUMBERS
F49620-97-1-0331

3484/WS
61103D

6. AUTHOR(S)
THOMAS E. DILLER

7. PERFORMING ORGANIZATION NAME(S) AND ADDRESS(ES)
VIRGINIA TECH
DEPARTMENT OF MECHANICAL ENGINEERING
BLACKSBURG, VA 24061-0237

8. PERFORMING ORGANIZATION REPORT NUMBER

9. SPONSORING/MONITORING AGENCY NAME(S) AND ADDRESS(ES)
AIR FORCE OFFICE OF SCIENTIFIC RESEARCH
801 N. RANDOLPH STREET, ROOM 732
ARLINGTON, VA 22203-1977

10. SPONSORING/MONITORING AGENCY REPORT NUMBER

11. SUPPLEMENTARY NOTES

12a. DISTRIBUTION AVAILABILITY STATEMENT
APPROVED FOR PUBLIC RELEASE, DISTRIBUTION IS UNLIMITED

12b. DISTRIBUTION CODE

13. ABSTRACT *(Maximum 200 words)*

This study is an investigation of the film cooling effectiveness and heat transfer coefficient of a two-dimensional turbine rotor blade in a linear transonic cascade. Experiments were performed in Virginia Tech's Transonic Cascade Wind Tunnel with an exit Mach number of 1.2 and an exit Reynolds numbers of 5x106 to simulate real engine flow conditions. The freestream and coolant flows were maintained at a total temperature ratio of 2 +0.4 and a total pressure ratio of 1.04. The freestream turbulence was approximately 1%. There are six rows of staggered, discrete cooling holes on and near the leading edge of the blade in a showerhead configuration. Cooled air was used as the coolant. Experiments were performed with and without film cooling on the surface of the blade. The heat transfer coefficient was found to increase with the addition of film cooling an average of 14% overall and to a maximum of 26% at the first gauge location. The average film cooling effectiveness along the chord-wise direction of the blade is 25%. Trends were found in both the uncooled and the film-cooled experiments that suggest either a transition from a laminar to a turbulent film regime or the regime or the existence of three-dimensionality in the flow-field over the gauges.

14. SUBJECT TERMS	15. NUMBER OF PAGES
	104
	16. PRICE CODE

17. SECURITY CLASSIFICATION OF REPORT	18. SECURITY CLASSIFICATION OF THIS PAGE	19. SECURITY CLASSIFICATION OF ABSTRACT	20. LIMITATION OF ABSTRACT
U	U	U	

Executive Summary

Four graduate students were supported at least in part on this AFOSR AASERT grant on "Film Cooling Visualization and Heat Transfer on Transonic Turbine Blades." Three completed M.S. degrees, while the fourth is currently working to complete a PhD.

MS degrees finished in 1999:

James Bubb
Dwight Smith
Hank Grabowski

Continuing PhD:

Andrew Nix

The attached report includes the main body of the theses by Bubb and Smith, which give the bulk of the detailed results. The work by Smith shows the film cooling effectiveness results and the change in heat transfer due to the presence of the coolant flow. The steady-state results are as expected at most locations on the suction surface of the blade. The heat transfer is increased by 14% to 25% across the locations studied. The film cooling effectiveness is an average of 25%. These results form the baseline for the unsteady research which was the focus of the accompanying project. The work by Bubb shows the effect of changing the pressure ratio, defined as the ratio of total pressure of the coolant flow to that of the freestream flow. Over a range of 1.02 to 2.0 (the nominal value is 1.04) the effect on film cooling effectiveness and heat transfer coefficient is small. This was not expected and shows that increasing the blowing over this range of values on the suction side is not recommended for surface heat transfer effects.

An Investigation of Heat Transfer Coefficient and Film Cooling Effectiveness in a Transonic Turbine Cascade

By
Dwight E. Smith

Thesis Submitted to
Virginia Polytechnic Institute and State University
in partial fulfillment of the requirements for the degree of

Master of Science

in

Mechanical Engineering

Thomas E. Diller, Chairman
Wing Ng
Joseph A. Schetz

March 28, 1999
Blacksburg, Virginia

Keywords: heat transfer, film cooling, and transonic turbine

An Investigation of Heat Transfer Coefficient and Film Cooling Effectiveness in a Transonic Turbine Cascade

Dwight Smith

Virginia Polytechnic Institute and State University, 1999

Advisor: Dr. Thomas E. Diller, Dr. Wing F. Ng, Dr. Joseph A. Schetz

(ABSTRACT)

This study is an investigation of the film cooling effectiveness and heat transfer coefficient of a two-dimensional turbine rotor blade in a linear transonic cascade. Experiments were performed in Virginia Tech's Transonic Cascade Wind Tunnel with an exit Mach number 0f 1.2 and an exit Reynolds numbers of $5x10^6$ to simulate real engine flow conditions. The freestream and coolant flows were maintained at a total temperature ratio of 2 ±0.4 and a total pressure ratio of 1.04. The freestream turbulence was approximately 1%. There are six rows of staggered, discrete cooling holes on and near the leading edge of the blade in a showerhead configuration. Cooled air was used as the coolant. Experiments were performed with and without film cooling on the surface of the blade. The heat transfer coefficient was found to increase with the addition of film cooling an average of 14% overall and to a maximum of 26% at the first gauge location. The average film cooling effectiveness along the chord-wise direction of the blade is 25%. Trends were found in both the uncooled and the film-cooled experiments that suggest either a transition from a laminar to a turbulent film regime or the existence of three-dimensionality in the flow-field over the gauges.

Table of Contents

Nomenclature

C	Specific heat (J/kg·K)
G	Gain (V/V)
L_{ss}	Total length of the suction side of the blade (m)
M	Mach number (-)
P	Pressure (psig)
R	Resistance associated with the temperature sensor of the HFM (Ohms)
Re	Reynolds number based on chord length of blade (-)
S	Sensitivity associated with the HFM ($\mu V/W/cm^2$)
T	Temperature (°C)
V	Voltage (volts)
h	Heat transfer coefficient ($W/m^2 \cdot °C$)
k	Thermal conductivity ($W/m^2 \cdot °C$)
q	Heat flux (W/cm^2)
r_c	Recovery factor for high-speed flows (-)
s	Distance measured from the stagnation point to some point along the suction side of the blade (m)
u_∞	Velocity at the edge of the film layer (m/s)

Greek

α	Thermal diffusivity (m^2/s)
δ	Material thickness through which heat is conducted (m)
η	Adiabatic film cooling effectiveness (%)
ρ	Density (kg/m^3)

Subscripts

HFS	Associated with the heat flux sensor
KUL	Associated with Kulite pressure transducers
R	Recovery
RTS	Associated with the resistance temperature sensor
aw	Adiabatic wall
c	Coolant
o	Total
w	Turbine blade wall

Chapter 1: Introduction

There is a strong demand in today's gas turbine industry for higher turbine inlet temperatures. The reason for this push is that higher turbine inlet temperatures can be translated into improved turbine efficiency.

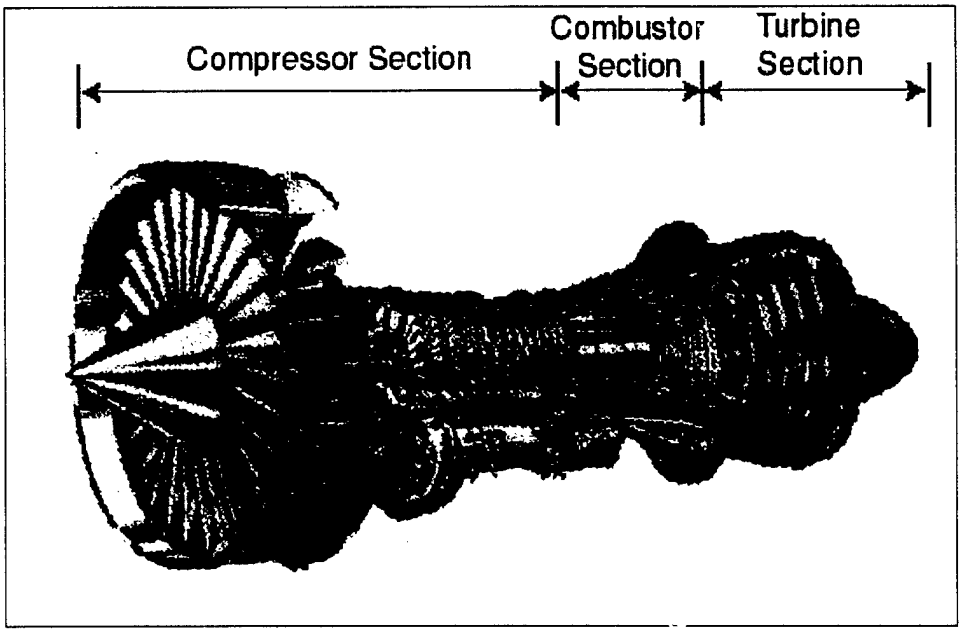

Figure 1: Typical Turbofan Engine

However, turbine inlet temperatures are limited by the thermal loads that the turbine blades are capable of withstanding. At present, the inlet temperatures to gas turbines are pushing the limits of the materials used in their construction. In order to maintain safety and to prolong the life of turbine blades, it has become necessary to protect them from the hot engine environments. One of the ways in which turbine blades are protected is through the use of film cooling. In film cooling, cool air is forced through holes on the surface of the blade. This air then forms a thin, protective layer

between the hot combustion gases and the surface of the blade. Because the air needed to cool the blades is drawn directly from the compressor section of a turbine, it is seen as a loss of work. Therefore, it is necessary to develop an understanding of how film cooling affects heat transfer into the blade in order to minimize the amount of air withdrawn from the compressor.

At present, analytical methods are limited in providing this information because of the complexities of the flow fields and interactions taking place. For this reason, experimental measurements must be used to determine heat transfer coefficients and film cooling effectiveness. In turn, this information can be used as a baseline for future computational studies.

Some of the things that are known to affect cooling films and heat transfer on turbine blades are shock and wake passing caused by the stators just upstream of the rotors, compressibility, curvature of the blade, and the size, chord-wise orientation and inclination of the cooling holes. There are many studies performed on flat plates which look at the effects these parameters have on film cooling, but the results from these studies are not always applicable to real engine conditions. Also, none of these flat plate studies investigated the unsteady effects of shocks and wakes on film cooling. The Virginia Tech Transonic Wind Tunnel is capable of studying both the steady and the unsteady effects of freestream turbulence and shock wave passing on the film cooling layer and the heat transfer into turbine blades.

The intent of this thesis is to investigate the steady heat transfer coefficient and the effectiveness of a film cooled turbine rotor blade with realistic geometry in flow conditions similar to those found in a real engine. Table 1 shows the parameters which

were used for the experiments. These values were chosen in order to simulate real engine conditions. This work will form the basis for future experiments which will look at the unsteady effects which shock wave passing and free stream turbulence have on the cooling films and heat transfer into the blade.

Table 1: Tunnel Parameters

Exit Mach No.	1.2
Exit Reynolds No.	5×10^6
Temperature Ratio ($T_{o,c}/T_{o,\infty}$)	2 ± 0.4
Pressure Ratio ($P_{o,c}/P_{o,\infty}$)	1.04
Freestream Turbulence Level	1 %

Chapter 2: Literature Review

In an attempt to provide information about the heat transfer into turbine blades which employ film cooling, many flat plate experiments have been performed. These experiments were easy to perform and allowed researchers to amass a great deal of information about the parameters that affect heat transfer into a film-cooled surface. A good compilation of the experimental work done on flat plates was put together by Goldstein (1971). These works were important beginnings, but the results can not describe actual engine flows because they lack curvature, cross- stream pressure gradients, and the highly accelerated flows seen on the pressure and suction sides of a turbine blade. The results of the flat plate work can provide insights into the heat transfer on the suction side, however, because the suction side flows are somewhat similar to flow over a flat plate.

Schwarz et al. (1990) investigated the effects of curvature and blowing ratio on the film cooling effectiveness of a convex surface, i.e. a surface similar to the suction side of a blade, and made comparisons to a concave surface. They found that curved surfaces had better film cooling effectiveness than flat plates. The reason for this is that the cross-stream pressure gradient acts counter to the lifting momentum forces of the jets and forces them to stay on or close to the surface of the blade. Also, Schwarz et al. found that at low blowing rates, film cooling is more effective on the suction side of the blade than on the pressure side. High injection rates on the suction side of the blade promote lifting of the coolant film from the surface and lessen the protection that film provides. This

work was an intermediate step between flat plates and investigations of heat transfer into realistic blade geometries.

Most of the work done with realistic blade geometries were short duration experiments which captured the transient surface temperature history. For short periods, the assumption of one-dimensional, semi-infinite conduction into the blade is valid for heat transfer into the blade. The solution for this case is well known and can be used to determine the heat flux into the blade since the temperature history is known. Several experiments were performed using this method of obtaining the surface heat flux.

Horton et al. (1985) investigated the heat transfer into a realistic turbine blade profile mounted in a linear cascade. Thin-film resistance sensors were used in a short duration blow down tunnel to capture the transient surface temperature history. The exit Mach number was 0.94 and the freestream to coolant temperature ratio was 1.3, so some attempts at matching real engine conditions were made as well. Air was used as the coolant on the blades. Horton et al. were able to obtain measurements of the heat transfer coefficient at several locations along both the pressure and suction sides of the blade.

In 1995, researchers at G. E. Aircraft Engines performed heat transfer measurements on a film-cooled inlet nozzle guide vane (NGV) in a linear cascade with realistic flow conditions [Abuaf et al., 1995]. Thermocouples embedded in a thin-walled turbine blade were used to measure the transient surface temperature. The exit Reynolds number was on the order of $3x10^6$, the freestream to coolant density ratio was 2, and the blowing ratio was varied between 1.5 and 2.7. Air was used as the coolant in their cooling scheme. Heat transfer coefficient and effectiveness profiles were obtained for both sides of the blade, but both profiles displayed noise in the results immediately

downstream of the cooling holes. Also in 1995, Ekkad et al. investigated the effects of freestream turbulence on the heat transfer into a film-cooled turbine blade. Thermotropic liquid crystals (TLC's) were used to obtain the transient surface temperature history. TLC's have an advantage over gauges in that they provide information over the entire surface to which they are applied, and not just to discrete locations. They concluded that high freestream turbulence leads to an increase in heat transfer coefficient.

Researchers at Oxford University used thin-film gauges to study the heat transfer into a heavily film-cooled NGV [Guo et al., 1996 and 1997]. There measurements were performed in an annular cascade with attempts made to simulate realistic engine conditions (13% freestream turbulence, $Re \cong 2x10^6$, $M \cong 0.96$). A mixture of SF_6 and Argon was used as a coolant. The heat transfer coefficient and film cooling effectiveness profiles were determined for the pressure side of the NGV.

In 1998, Drost et al. used TLC's to record the transient surface temperature history of an NGV airfoil exposed to a step input in heat transfer while in a linear cascade. They used a foreign gas as a coolant to obtain a realistic density ratio. They concluded that the film cooling effectiveness was higher near the cooling holes and that the mainstream turbulence level had a weak effect on suction side effectiveness, but that it increased suction side heat transfer coefficients.

All of these experiments were performed in such a way that the heat flux was measured indirectly using the transient surface temperature history. Researchers at Virginia Tech are using a thin-film gauge which is capable of direct measurements of both the local heat flux and surface temperature simultaneously [reference Drew,

Holmberg, Doughty]. This gauge, the HFM-7 is the newest version, will be used in the present work to investigate heat transfer into a film-cooled transonic turbine inlet NGV.

Chapter 3: Experimental Setup and Instrumentation

The experiments that were investigated in this study were all performed in the Virginia Tech Transonic Wind Tunnel. This tunnel is an intermittent blow-down facility with an open discharge, and it can be used for both transonic and supersonic testing. The compressor system feeds a large volume of pressurized air into a storage tank, and on-off valves determine whether flow is directed into the supersonic or the transonic facilities. A fast-acting control valve regulates the release of the pressurized air into the test section of the transonic portion of the tunnel.

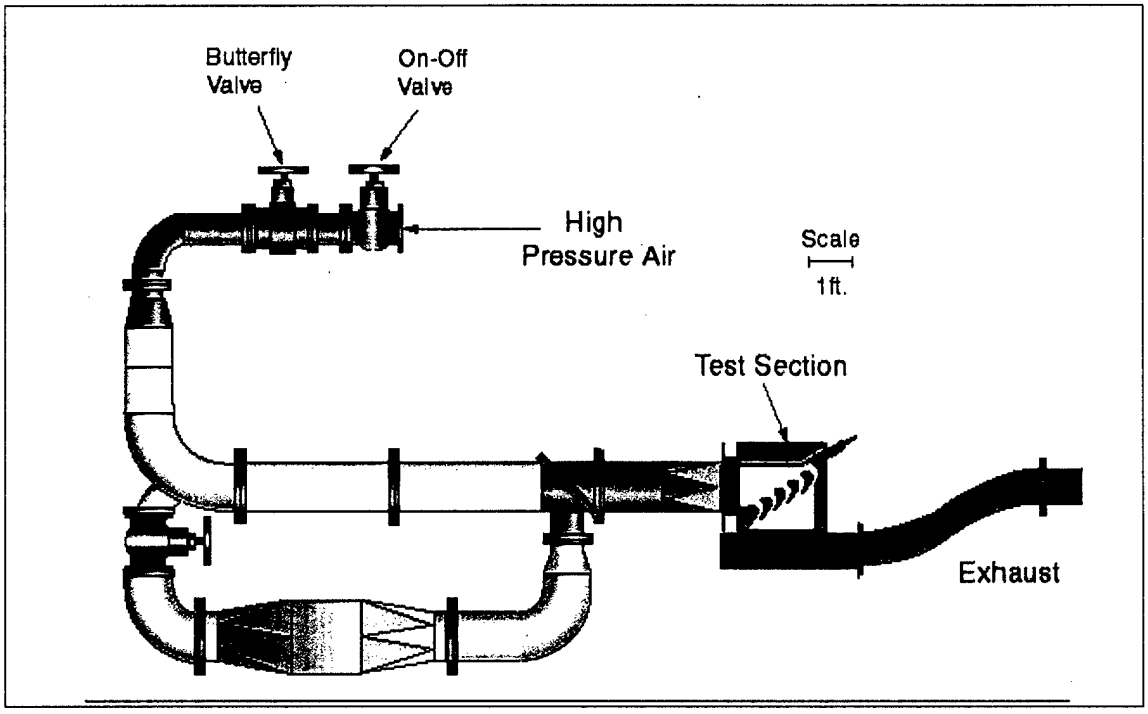

Figure 2: Schematic of Transonic Cascade Wind Tunnel

3.1 Cascade Wind Tunnel Compressor System

The compressor, which feeds the cascade wind tunnel, is an Ingersoll-Rand model HHE 334 four-stage, reciprocating compressor that is capable of pressurizing air up to 750psig. The pressurized air is circulated through a dryer to remove moisture and fed into a storage tank. Measurements have shown that the relative humidity of the air leaving the dryer is less than 7%. The tank is connected to the cascade wind tunnel by a system of 14" diameter, Schedule 30, carbon steel pipes. This system of pipes also includes an on-off valve and a fast-acting control valve. The control valve is a butterfly valve that is regulated by a feed-forward program that monitors the tunnel's total pressure and temperature as well as the tank pressure, and then calculates the optimum valve position to maintain the desired flow conditions. The control program attempts to maintain the total pressure at the inlet of the test section, and thus the test section's inlet Mach number, to within 10% of the set point. This program, named WINDN3.C, was written in Turbo-C and is stored on the tunnel control computer. The mass flow rate of air through the tunnel is approximately 10 kg/s and the typical run time is 30 seconds.

3.1.1 Heated Flow

Some of the experiments performed in this study require that the mainstream flow be much hotter than ambient conditions in order to simulate the temperature ratios that might be seen in actual engine conditions. The cascade wind tunnel has a closed loop heating system, which allows for such heated mainstream flows. A schematic of the system is shown in Figure 3.

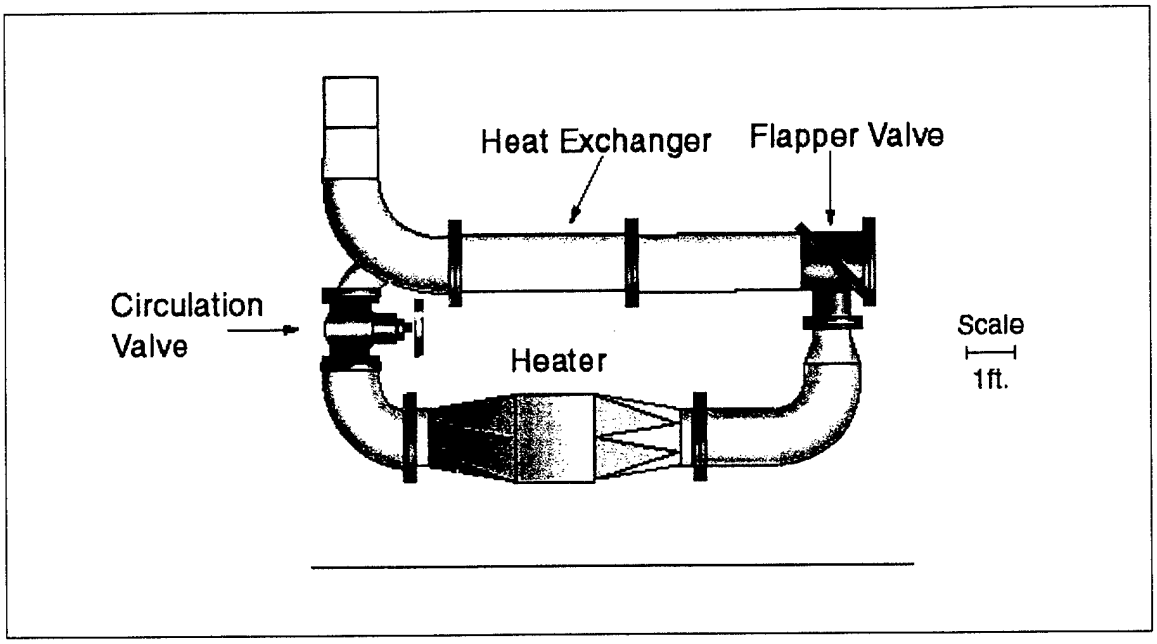

Figure 3: Circulation Loop for Heated Flows

The heating system is an insulated loop of pipe closed off from the tunnel supply and the test section by three valves. The circulation valve is opened in order to begin preheating. Once the flapper valve and the upstream on-off valve are shut, two 36kW heaters are turned on and supply energy to the air. A fan forces the heated air to circulate through the loop and over a bank of copper tubes. There are 350, one-meter-long, copper tubes in the bank. A thermocouple mounted in the flow monitors the temperature of the air. The air in the loop is heated up to 20°C above the desired starting temperature and allowed to reach equilibrium before the two valves are opened and testing is done. When air flows over the bank of copper tubes, it acts as a heat exchanger and transfers energy to the mainstream flow. For the experiments in this investigation, the desired starting total temperature for heated flows was 100°C and there was typically a drop in temperature of 70°C over the course of a run.

3.1.2 Coolant Supply System

The coolant supply system which supplies air to the film cooling holes is a separate, smaller version of the system that supplies air to the mainstream flow. A schematic of the coolant supply system is shown here in Figure 4.

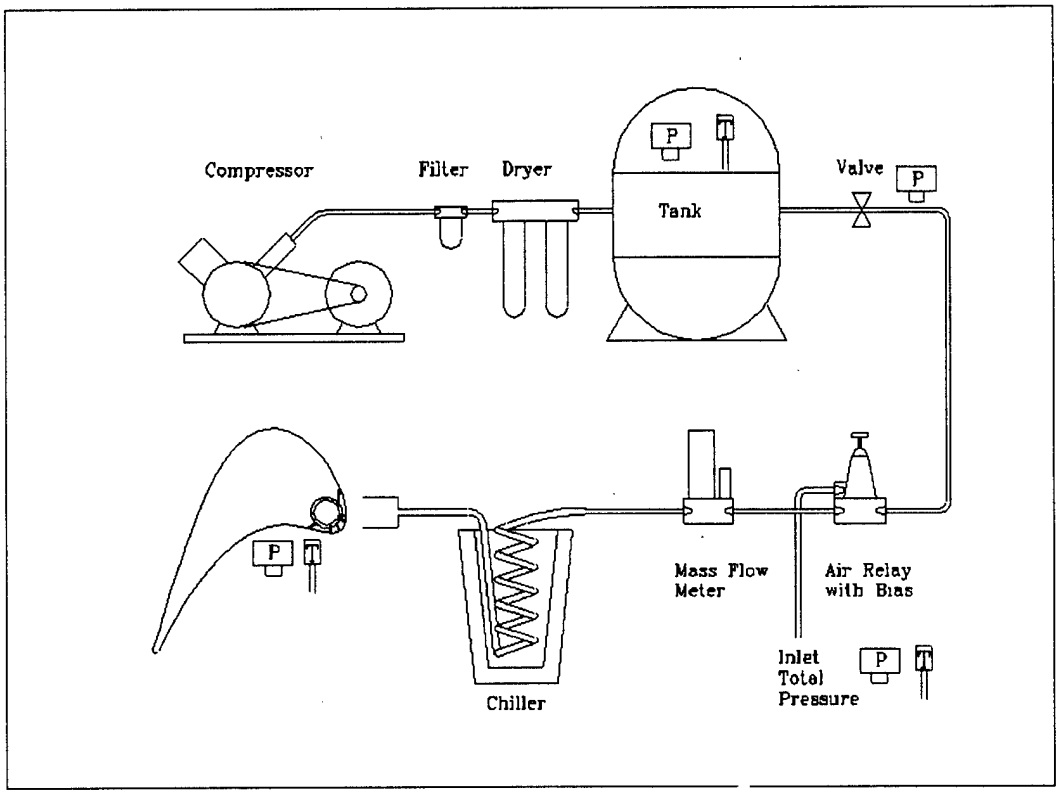

Figure 4: Schematic of Coolant Supply System

An Ingersoll-Rand 5Hp, two-stage, reciprocating compressor is used to supply pressurized air up to 150 psig at a flow rate of up to 25 SCFM. This air then flows through a dryer that removes the moisture from the air before it is stored in a large tank. Hereafter, this tank will be referred to as the coolant supply tank to distinguish it from the tank used to provide the mainstream flow. The relative humidity of the air leaving the dryer is less than 4%. A Marsh-Bellofram type 72 air relay is used to regulate the pressure of the air released from the storage tank. The air relay uses the mainstream

flow's total pressure measured just upstream of the test section as a reference and offsets it appropriately so that the desired plenum to tunnel total pressure ratio may be maintained. A plenum to mainstream pressure ratio of 1.04 was used in this work. The mass flow of the air supplied to the plenum is measured using an orifice plate with a calibration provided by the manufacturer. Usually, the mass flow was approximately 15 g/s. A heat exchanger, which uses liquid nitrogen as the coolant, is employed to lower the temperature of the air entering the coolant holes of the blade.

3.2 Test Section

The test section that contains the turbine blades investigated in this study was made from aluminum. Clear, acrylic windows were used for the endwalls so that flow visualizations could be made through optical means such as shadowgraphs and Schlieren photographs. Shadowgraphs can show extreme gradients in density such as those caused by shocks; Schlieren photography can capture weaker density gradients, and so can give a better picture of flow phenomena within the boundary layer. The actual test section and a schematic are shown side by side in Figure 5.

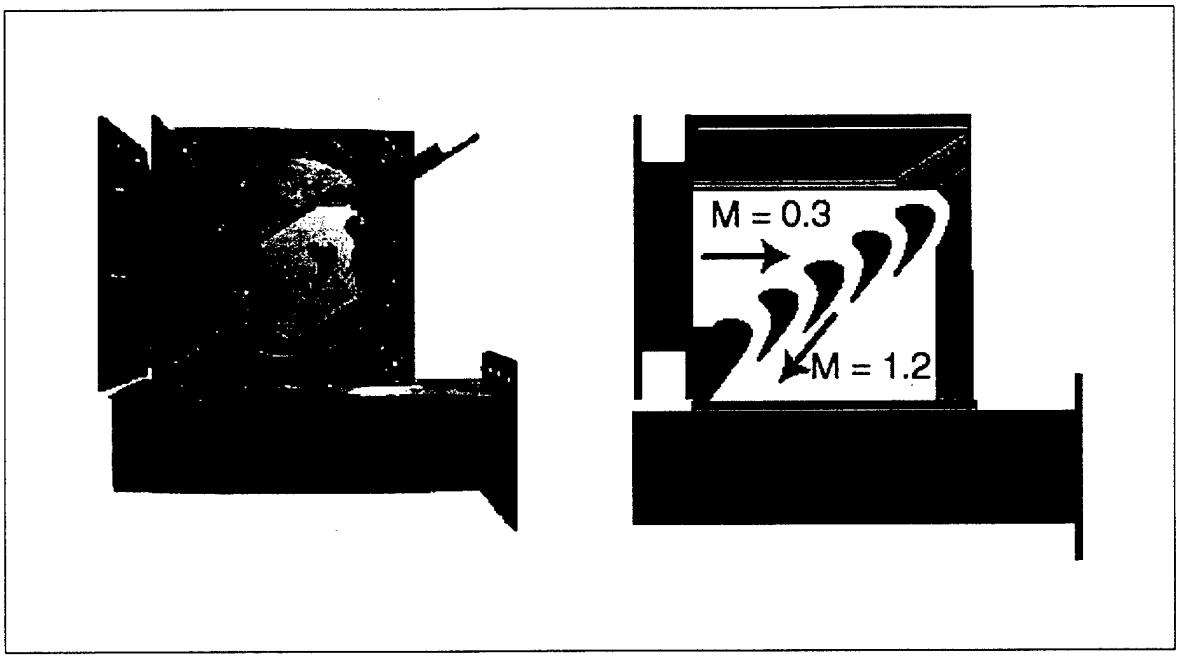

Figure 5: Picture and Schematic of Test Section

The test section is located just downstream of a nozzle that accelerates the flow up to Mach 0.3 prior to entering the test section. After entering the test section, the flow then passes over a set of turbine inlet rotor blades. There are four full blades and two half-blades contained in the test section; a total of five flow passages. The blade that was instrumented and used in this study is the second full blade from the bottom left in Figure 5, and it is shown darkened. The flow accelerates up to as much as Mach 1.2 as it passes over the blades and exits the blade passages. The blades are fixed into the endwalls at a fixed incidence angle of 58 degrees.

3.2.1 Instrumented Blade

The turbine blades used in this work are manufactured according to a generic, high-turning rotor blade design donated by General Electric. A showerhead cooling scheme is employed near the leading edge of the instrumented blade for film cooling. The entire blade can be seen in Figure 6.

Figure 6: Picture of Entire Instrumented Blade

Six rows of cooling holes are located near the leading edge of the blade. Beginning approximately 25 mm after the last row of cooling holes on the suction side, six sets of gauges were installed on the blade. Each set of gauges is composed of a heat flux microsensor (HFM), a surface thermocouple, and a Kulite pressure transducer. In order to install all of this instrumentation without unnecessary disruption of the blade surface the blade was made in two pieces, a portion of the suction side and a pressure side. This method of manufacturing allowed the external blade profile to be maintained while allowing room for the wiring of instrumentation within the blade.

It is important to maintain the external profile of the blade in order to avoid affecting the air as it flows over the surface of the blade. The blade has a six-inch span and a chord length of 4.5 inches. With such a large blade, it was possible to design the two pieces of the blade such that they joined in areas where there was not a lot of curvature. The two pieces were manufactured separately using a wire EDM. The two

junctions were polished to form a smooth surface. A schematic showing the arrangement and shape of the two pieces can be seen in Figure 7.

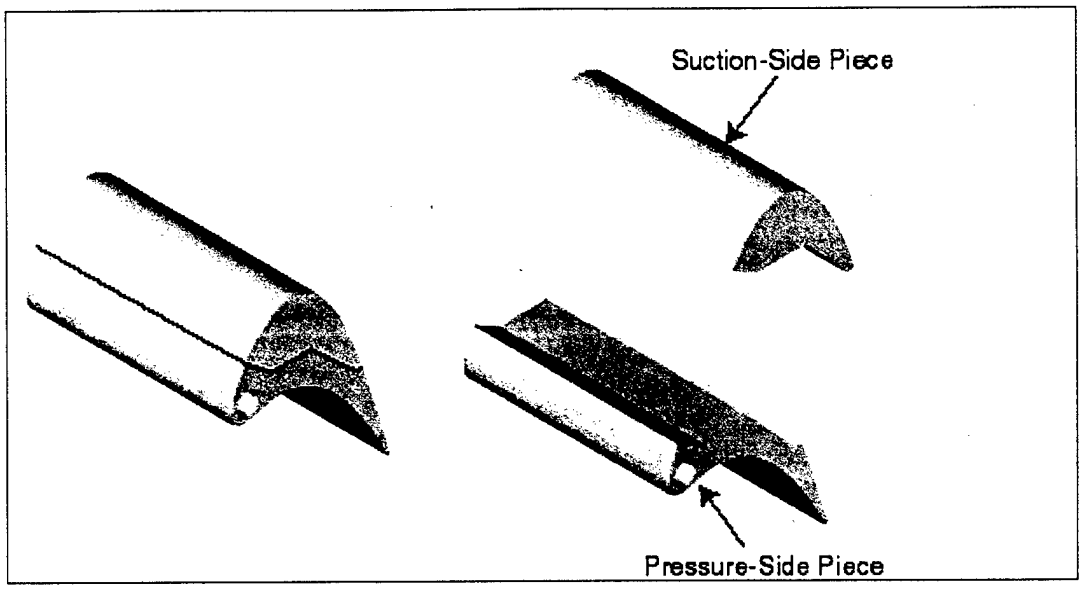

Figure 7: Schematic of Blade Manufacturing

All of the pressure side and a portion of the suction side are contained in the lower piece of the blade, which will hereafter be referred to as the pressure-side piece. The other piece of the blade, containing the rest of the suction side, will be referred to as the suction-side piece.

3.2.1.1 Pressure Side

The pressure-side piece of the blade contains the plenum and all of the coolant holes that produce the film. A picture of the pressure side can be seen in Figure 8.

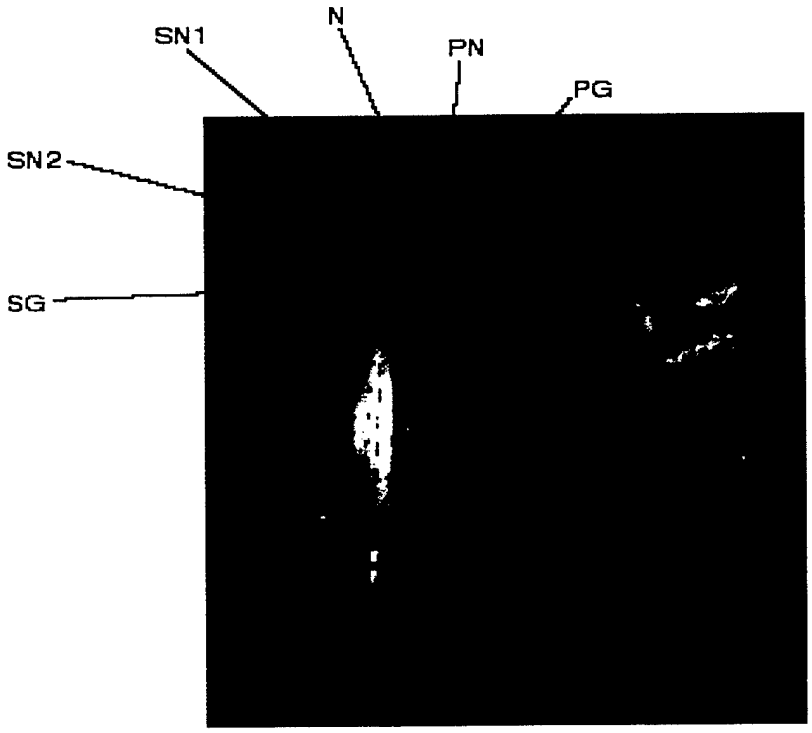

Figure 8: Pressure-side Piece of Instrumented Blade

A plenum designed for minimum pressure change across its length is used to supply air to the cooling holes. The plenum is insulated with polyethylene sulfone (0.12 W/m K) so that the cold air used for cooling does not affect the blade temperature which, in turn, could affect the air temperature. The cooling holes are staggered and discrete, which is similar to the blade cooling schemes found in actual engines. The four rows of holes nearest the leading edge all have 90 and 30-degree streamwise orientation and spanwise inclination angles, respectively. The last two rows of holes, one on either side of the pressure side piece, are in the streamwise direction but have 45-degree inclination angles. A schematic of the alignment of the cooling holes can be seen in Figure 9.

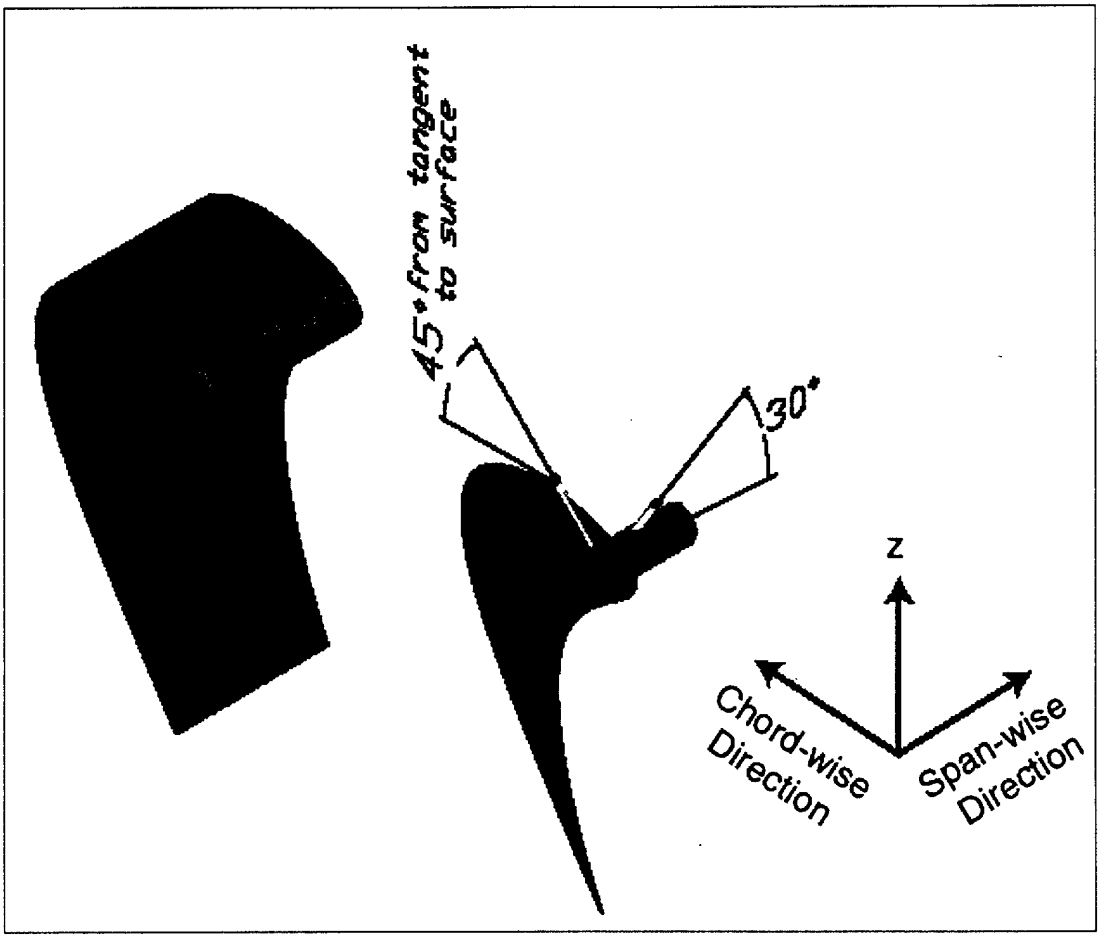

Figure 9: Schematic of Coolant Hole Alignment

Thermocouples are inserted into the second hole from the far end wall on each row of cooling holes in the blade in order to measure the temperature of the coolant. The thermocouples are of the type K, and were ordered from Omega. A static pressure tap is located in the hole nearest the far end wall of each coolant row so that the local freestream Mach number can be determined.

3.2.1.2 Suction Side

The suction-side piece contains the majority of the instrumentation used on the blade. Six triplets of gauges are staggered span-wise and chord-wise along its surface. This arrangement can be easily seen in Figure 10.

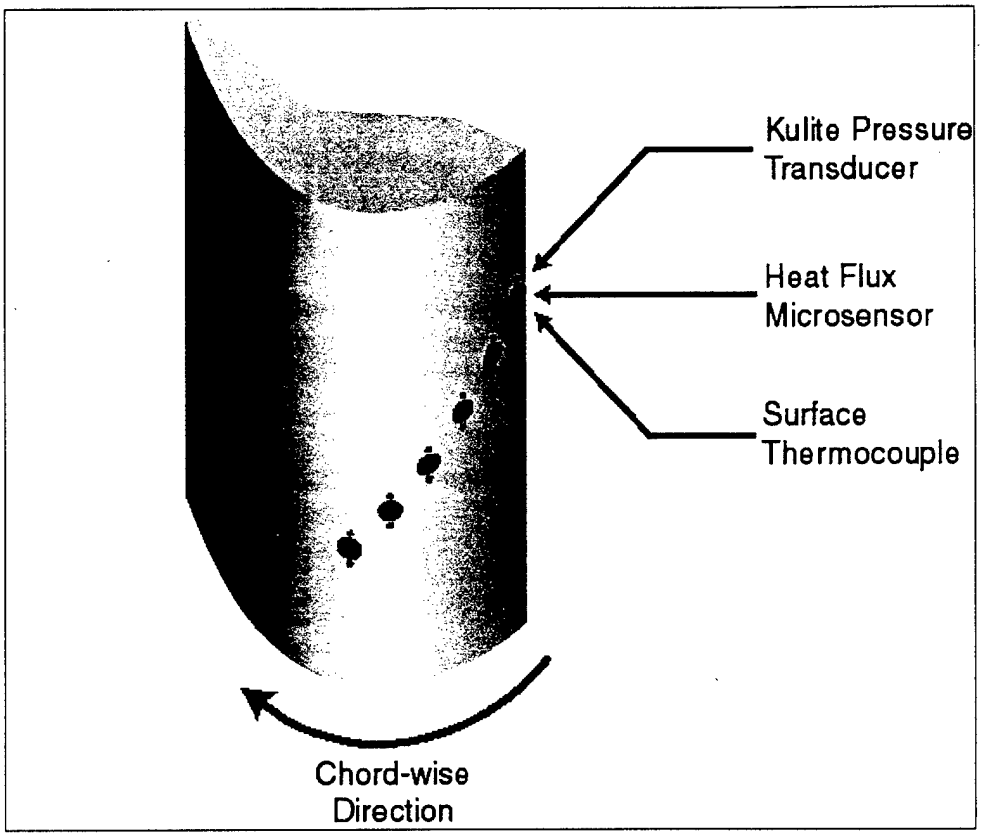

Figure 10: Suction-side Piece of Instrumented Blade

Each triplet of gauges is composed of a HFM, a surface thermocouple and a Kulite pressure transducer. All of the instrumentation was pressed into the blade so that there would be a good thermal contact between the blade material and the gauges. Using the six-inch blade, the curvature on the suction side is not extreme and installing the gauges made only very small disruptions to the surface. However, to avoid the downstream effects of the previous gauges, subsequent gauges are staggered in the span-wise direction. The sets of gauges were also staggered chord-wise so that the variation of heat transfer and effectiveness could be seen along the blade.

3.3 Instrumentation

3.3.1 Data Acquisition

Data was taken as input on a National Instruments' AT-MIO-16XE-50 acquisition board. This board can sample at rates of up to 20,000 samples per second, but has only eight differential channels. In order to record all of the data that were required for this study, two National Instrument's AMUX-64T analog multiplexers were used to expand the number of channels that could be sampled. A Labview program was written in order to set data acquisition parameters and to record the data to a file.

3.3.2 Heat Flux Microsensor

All heat flux measurements in this work were taken using a commercial heat flux microsensor (HFM) produced by Vatell Inc. The HFM-7, the gage used in these experiments, is composed of two separate sensors: a thin-film resistance temperature element and a heat flux microsensor. The HFM-7 was chosen because future work on this project will involve investigating the effect of shock wave interaction with the film-cooling boundary layer. The entire shock event is only about 50 μs, so the gage chosen had to have a very fast time response. The HFM-7 was used because it is a thin-film sensor with a time response on the order of 10μs, so it is capable of capturing the effect of shock wave passing on heat transfer and blade temperature.

Blade temperature is measured by the HFM-7 using a resistance temperature sensor (RTS) which is sputtered onto the surface of the gage. The RTS is a thin-film element that is only 2 microns thick and is deposited in a circular pattern around the heat flux sensor. The RTS operates on the principle that the resistance of metals changes in a predictable way with temperature. A current of 0.1 mA is used to excite the RTS. Over a

range of temperatures from 0°C – 250°C, the change in resistance is nearly linear. Outside of this range, the change in resistance can still be estimated using a cubic polynomial of the form,

$$T(R) = a \cdot R^3 + b \cdot R^2 + c \cdot R + d \tag{1}$$

Where R is the measured resistance in ohms
a, b, c, and d are the coefficients of the polynomial

The polynomial coefficients are determined through a calibration performed by the manufacturer. The coefficients for the gauges used in this work can be seen in Appendix C. The experiments performed in this work were all within the range of temperatures for which the change in resistance is still linear, so only the linear coefficients c and d were used for the RTS calculations. Changes in temperature are dependent upon changes in resistance, so it is important that both the initial temperature, T_o, and the initial resistance, R_o, be known. T_o is measured using a thermocouple on the blade, and R_o is calculated using the equation,

$$R_o = e \cdot T_o + f \tag{2}$$

where e and f are coefficients determined from the calibration of the RTS. The resistance of the RTS at other temperatures is then calculated by,

$$R = \frac{V_{RTS}}{I_{RTS} \cdot G_{RTS}} + R_o \tag{3}$$

Where V_{RTS} is the output of the RTS in μV
I_{RTS} is the excitation of the RTS in amps
G_{RTS} is the gain of the amplified RTS signal

Temperature is then calculated using equation (1). This temperature is used when calculating the heat flux.

The heat flux sensing element (HFS) is used to measure the flow of heat into and out of the blade. The HFS is a passive differential thermopile sensor made up of 280 thermocouple pairs. Each of the thermocouple pairs consists of a Nichrome/Constantan thermocouple junction. Although the voltage output of this particular thermocouple junction is small, it was chosen because it can withstand temperatures up to 1000°C. The thermocouple junctions were deposited in a serpentine pattern on the surface of the gage. The HFS operates on the principle that the heat flux through a material, assuming one-dimensional conduction and steady state conditions, is proportional to the temperature difference across the material. This principle is illustrated in Fourier's equation,

$$q = \frac{k}{\delta}(T_1 - T_3) \tag{4}$$

Where
- q is heat flux (W/cm^2)
- k is the thermal conductivity (W/cm^2 C)
- δ is the thickness (cm)
- T_1 is the substrate temperature (°C)
- T_3 is the insulated surface temperature (°C)

A schematic of one of the thermocouple junction pairs in the HFS can be seen in Figure 11.

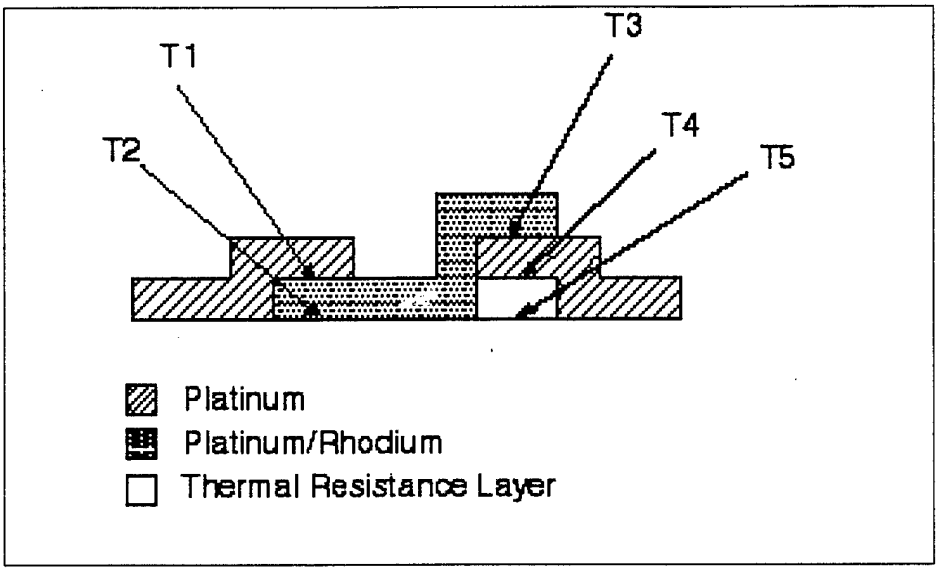

Figure 11: Schematic of HFS Thermopile

One junction of each thermocouple blade is sputtered onto the aluminum nitride substrate and a thin layer of material with a low thermal conductivity insulates the other junction. When heat flows into the gage, this thermal resistance causes the insulated junction to reach a higher temperature than that of the junction deposited directly onto the high conductivity substrate. It is assumed that the high conductivity substrate has a uniform temperature (T2 = T5). The temperature difference across the thermal resistance layer is proportional to the voltage output across the two thermocouple junctions. Heat flux into the blade will result in a positive voltage, and flux out of the blade will cause a negative voltage. The sensitivity of the HFS is itself dependent upon temperature, so the temperature measured by the RTS is used to correct the output of the HFS.

The heat flux that passes into the HFS sensor is calculated using the following equation,

$$q = \frac{V_{HFS} / G_{AMP}}{S_T} \tag{5}$$

Where q is the heat flux in W/cm^2

V_{HFS} is the output voltage in μV
G_{AMP} is the gain of the amplified signal
S_T is the temperature dependent sensitivity

S_T, the temperature dependent sensitivity, is determined during the calibration of the HFS. The sensitivity of the HFS varies linearly with temperature and is given by the equation,

$$S_T = g \cdot T + h \tag{6}$$

Where g is the change in sensitivity with temperature ($\mu V/W/cm^2/°C$)
h is the HFS sensitivity at room temperature ($\mu V/W/cm^2$)

The coefficients g and h in the equation above are usually provided by the manufacturer. For the gauges used in this work, however, the sensitivity coefficient at room temperature was found using a transient calibration technique which is described in Appendix A. The sensitivity coefficients for each gauge in this work are listed in Appendix C. The change in sensitivity of the HFS with temperature is small, usually on the order of $\mu V/W/cm^2/°C$, so the coefficient g was considered to have a negligible effect. The temperature used in the above calculation is determined from the RTS. Since both sensors are on the same gage and receive the same incident flux, the temperature recorded by the RTS is the result of the heat flux measured by the HFS.

3.3.3 Kulite Pressure Transducer

Kulite XCQ-062-50 high-frequency transducers were used to take some of the pressure measurements used in this study. This gage uses a diaphragm connected to a piezo-electric crystal to generate a voltage in response to pressure differences across the diaphragm. A small metal screen was used to prevent flying particles in the mainstream flow from damaging the transducer. The gages are 1.7mm in diameter and have temperature compensation.

Pressure is directly translated into voltage by the crystal, so fast time responses of up to 100 kHz are possible if the Kulite is unscreened and up to 25 kHz with the screen in place. The voltage output of the Kulite is linear in proportion to the pressure it experiences. The typical value is about 2 mV/psi. Pressure is calculated from the Kulite output using the following equation,

$$P = \frac{V_{KUL}}{S_{KUL} \cdot G} \tag{7}$$

Where P is the pressure in psig
S_{KUL} is the Kulite sensitivity in mV/psi
G is the gain of the amplified signal

All of the Kulites used in this work were amplified with Measurement Group 2310 amplifiers set on a gain of 100V/V.

3.3.4 Amplifiers

3.3.4.1 Amp-6

The voltage output signals from both the RTS and HFS sensors were amplified with the AMP-6 amplifier, which is produced by Vatell, Inc. for use with the HFM-7 gage. A single LEMO connection on the AMP-6 takes input from both of the sensors on the gage. The AMP-6 also supplies a constant excitation current of 0.1 mA to the RTS and has channel specific gains. The amplifier is allowed to warm up at room temperature before the outputs of the two sensors are "zeroed."

In the case of the RTS, this means that a potentiometer is set to read the same resistance as that of the RTS at room temperature. Any changes in resistance caused by fluctuating temperatures are referenced to this "zeroed" resistance. The AMP-6 has gains of 1, 100, 200, and 500 for the amplified RTS signal.

For the HFS, another potentiometer is used as an offset to reduce the voltage output to zero. This is done when the gage and its surroundings are at the same temperature and no heat flux is incident on the blade. The AMP-6 has gains of 1, 100, 500, 1000, and 5000 for the HFS.

3.3.4.2 Measurements Group 2310

All measurements taken with the Kulite pressure transducers were amplified with a Measurements Group 2310 amplifier. The 2310 is a multi-channel amplifier designed for use with strain gages inputs—foil or piezo-resistive based. Excitation voltages can be provided from 0.5 Vdc up to 15 Vdc, and the gain of the output signal can be set from 1 to 11,000. The 2310 amplifier was allowed to warm up before the bridge was balanced.

3.4 Experimental Setup

3.4.1 Uncooled Blade

3.4.1.1 Overview

In order to understand how film cooling affects the turbine blade used in this work it was necessary to first determine the steady heat transfer coefficient profile in the streamwise direction without film cooling. Once obtained, this profile was used as a basis of comparison for the cases which are performed with film cooling present. This case (steady h w/o film cooling) was performed in the Virginia Tech Transonic Wind Tunnel, an intermittent blowdown facility which discharges to atmosphere. For these tests, a heated mainstream flow was used.

3.4.1.2 Setup

The instrumented blade described in section 3.2.1 was inserted into the test section, and the entire assembly was placed into the transonic wind tunnel. Although no film cooling was used during the actual run, the coolant supply system was connected to the plenum chamber of the instrumented blade. The coolant system was used to cool the blade down before performing experiments. Data was recorded on a computer.

3.4.1.3 Procedure

The instrumented blade was placed into the cascade test section in order to perform steady heat transfer measurements. The tunnel's mainstream air flow was heated up to 100°C as described earlier in the section on heated flow. The coolant supply compressor system was started and used to pump air into the coolant supply storage tank until the tank pressure reached 170 psig. Liquid nitrogen was released into the heat exchanger until it was approximately half-full. The instrumented blade was cooled down to 0°C using cold air from the coolant supply tank which was allowed to flow through heat exchanger and into the plenum and cooling holes. Once the blade reached zero, the coolant supply system was disconnected and a plug was placed into the plenum of the instrumented blade. The plug prevented the mainstream flow from entering the plenum through the coolant holes nearest the leading edge and blowing out the holes that are farther away. The tunnel control program was started, and separate, but simultaneous, time resolved heat transfer and temperature measurements were taken. The data produced by the six sets of gages staggered in the chord-wise direction along the instrumented blade was recorded to be analyzed later.

3.4.2 Film-cooled Blade (Cold Coolant)

3.4.2.1 Overview

The steady heat transfer coefficient profile along a turbine rotor blade was determined in these tests, which were performed in the Virginia Tech Transonic Cascade Wind Tunnel facility. The heat transfer coefficient is used to help determine the chord-wise variation of the adiabatic film cooling effectiveness. These two pieces of information, h and η, will also be used in future experiments that investigate the unsteady effects of shock wave passing on the film cooling of turbine blades. A heated mainstream flow was passed over an instrumented turbine rotor blade that had a showerhead film-cooling scheme.

3.4.2.2 Setup

The instrumented turbine rotor blade was inserted into the aluminum test section and the test section was placed into the transonic blowdown facility. Film cooling was used in these tests, so the coolant supply system was connected to the plenum chamber of the instrumented blade. The coolant system was used to cool down the blade before performing these experiments.

3.4.2.3 Procedure

The instrumented blade was inserted into the test section of the linear cascade in order to perform steady heat transfer experiments with film cooling. The tunnel was preheated to 100°C as described in the section on heated flow. The coolant supply compressor system was started and used to pump air into the coolant supply storage tank until the tank pressure reached 170 psig. Liquid nitrogen was released into the heat exchanger until it was approximately half-full. The instrumented blade was then cooled down to 0°C using air from the coolant supply tank which was allowed to flow through

the heat exchanger, become cold, and then flow into the plenum and cooling holes. The difference of the coolant total pressure in the plenum to the ambient total pressure was set to a nominal value of 2.4, using the air relay described in section 3.1.2. This was done before the tunnel's mainstream flow was started. This pressure difference between the coolant and the ambient air was determined through trial and error to give the desired coolant to freestream total pressure ratio of 1.04 once the tunnel's mainstream flow was started. Once these conditions had been reached, the tunnel control program was started and separate, simultaneous measurements of heat flux and temperature were taken. Data were collected from a set of six runs with film cooling.

3.4.3 Film-cooled Blade (Ambient Coolant)

3.4.3.1 Overview

Tests were performed in the Virginia Tech Transonic Wind Tunnel to determine the heat transfer coefficient profile generated on a turbine rotor blade with film cooling when the temperatures of the mainstream flow and the coolant are approximately the same. The heat transfer coefficient used in calculating convection heat flux is a proportionality constant that is used to separate the effects of temperature and flow phenomena on heat transfer. The results from these tests will give an idea of how good the assumption is that the effects of flow phenomena on convection heat transfer are contained within the heat transfer coefficient.

3.4.3.2 Setup

The instrumented blade was inserted into the test section and the entire assembly was placed into the transonic wind tunnel. The coolant supply system was connected to the plenum of the instrumented blade and used to cool down the blade before performing

the tests. The storage tank was loaded up to 170 psig. The mainstream flow was not heated for these experiments.

3.4.3.3 Procedure

The instrumented blade was placed into the cascade test section in order to perform steady heat transfer measurements with ambient temperature air as the coolant. The tunnel's mainstream air flow was not heat and allowed to remain at ambient temperature in order to accomplish this. The coolant supply compressor system was started and used to pump air into the coolant supply storage tank until the tank pressure reached 170 psig. Liquid nitrogen was released into the heat exchanger until it was approximately half-full. Air was allowed to flow from the coolant supply storage tank, through the heat exchanger, and then into the plenum and out the cooling holes. Once the instrumented blade reached zero, the coolant supply system was temporarily shut down while the copper tubing which transported the cooling air from the heat exchanger to the plenum was warmed using a heat gun. After the condensation build-up had been removed and the tubing had been warmed, the heat exchanger in the coolant supply system was bypassed and ambient temperature air was sent to the plenum chamber of the blade. The tunnel control program was started, and separate, but simultaneous, time-resolved heat transfer and temperature measurements were taken. The data used in this study were collected from various gauges over four runs made with film cooling where the injected fluid was at the same temperature as the mainstream flow.

Chapter 4: Evaluation of Test Section

4.1 Overview

The blade geometry used in this study was a generic design which was donated by GE along with their analytical predictions of what the flow field surrounding the blade should be. Before any serious testing could be done, it was necessary to determine what the actual flow field looked like and whether it matched the prediction. Also, the extent to which the endwalls influenced the flow over the blades and knowing what the cooling film looks like are both important. To get this information, several flow visualization techniques were used.

4.2 Oil Flow Visualization

An oil flow visualization was used to capture the disturbed flow near the endwalls. In Figure 12 the boundary layer induced by the end-wall can be seen. The endwall vortices grow quickly along the blade, but the six-inch span of the blade used is large enough that the disturbed flow does not pass over the area where the blade has been instrumented. The blade was instrumented in a 3.5 inch interval centered on the middle of the blade. This lies between the streamlines in the oil flow visualization which indicate the locations of the end-wall vortices. Figure 12 shows that the heat transfer measurements taken in this study should not be affected by the disruptions near the endwalls

Figure 12: Picture of Surface Oil-flow Visualization

4.3 Schlieren and Shadowgraph Photography

Ensuring that the flow was periodic is also very important. To resolve this question, Schlieren photographs were taken of the blade passages. The test section contains four full blades and two half blades, or five flow passages. Figure 13 shows a Schlieren photograph taken of the passage above the suction side of the instrumented blade. This picture shows that there is periodicity in the blade passages and also displays the expected trailing edge shock. Several pictures were taken and the shock angle remained constant and consistent with a maximum speed of Mach 1.4 before the shock. This indicates that the tunnel facility is capable of producing very repeatable flow conditions.

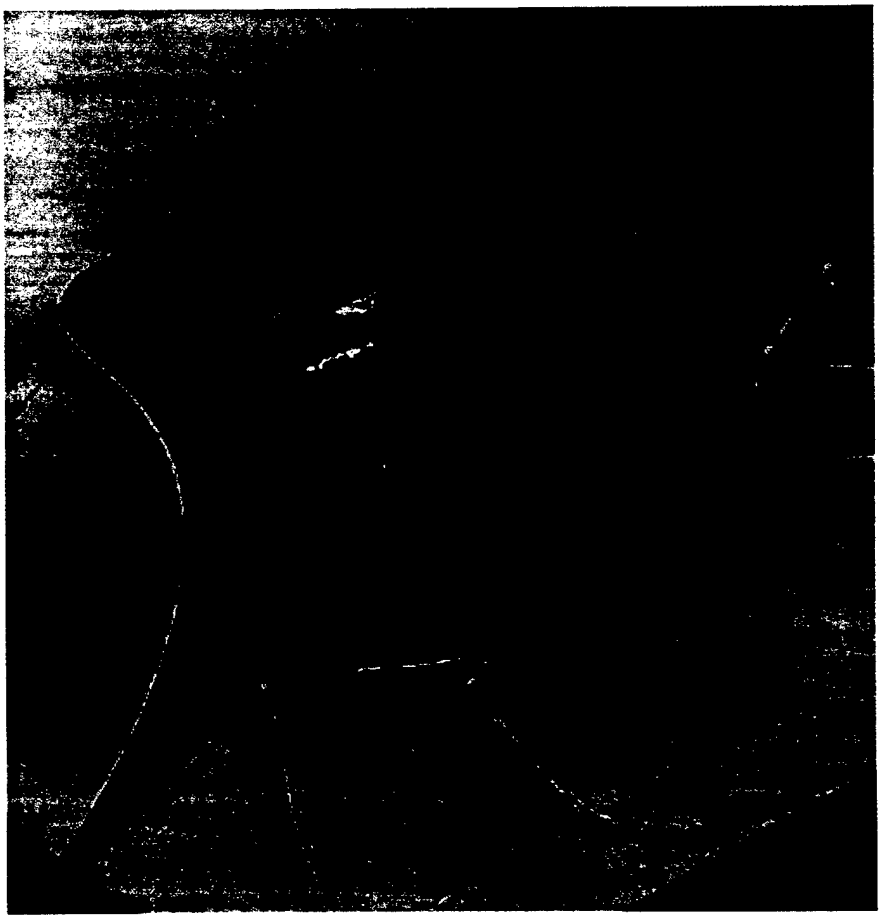

Figure 13: Schlieren Photograph of Flow in Blade Passages

Shadowgraph photography was used to examine the flow generated when the cooling system was employed. Figure 14 shows a shadowgraph of the instrumented blade's leading edge and suction side with coolant injection into the boundary layer. From this picture it can be seen that the stagnation point on the leading edge forces the jets from coolant holes along the nose to fold over onto the pressure side of the blade. Therefore, the coolant film present on the suction side of the blade is the result of only three rows of coolant holes. This shadowgraph shows that there is definitely a film present on the suction side and that it is attached. Turbulent cell structures can be seen in the film cooling layer, but it should be noted that this is an average across the blade.

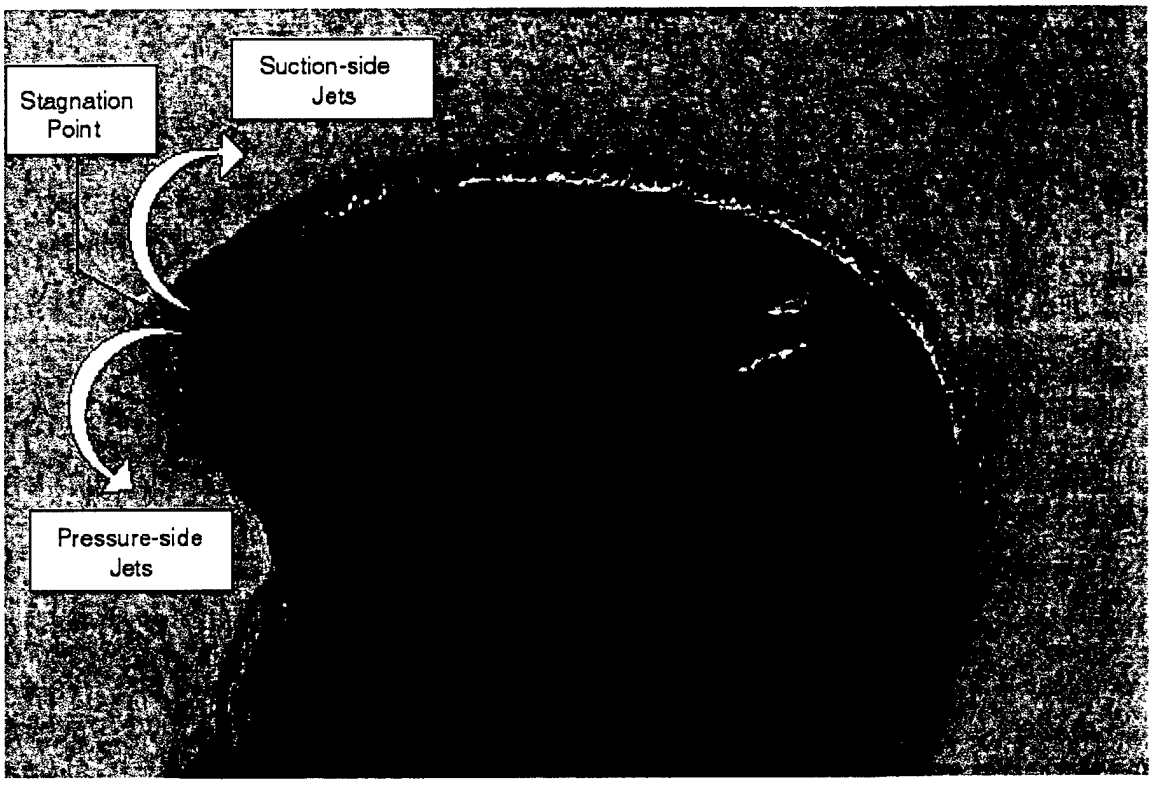

Figure 14: Shadowgraph of Cooling Film on Blade

4.4 Static Pressure Measurements

In order to check the actual flow field against the analytical prediction, static pressure measurements were taken using the Kulite pressure transducers which were spaced along the blade as was shown in Figure 10. Using these measurements it was possible to determine the chord-wise Mach number profile and to compare it with the predictions from GE. Figure 15 shows the actual Mach number profile along with the predicted values. The actual profiles are within 10% of the predicted profile at all locations.

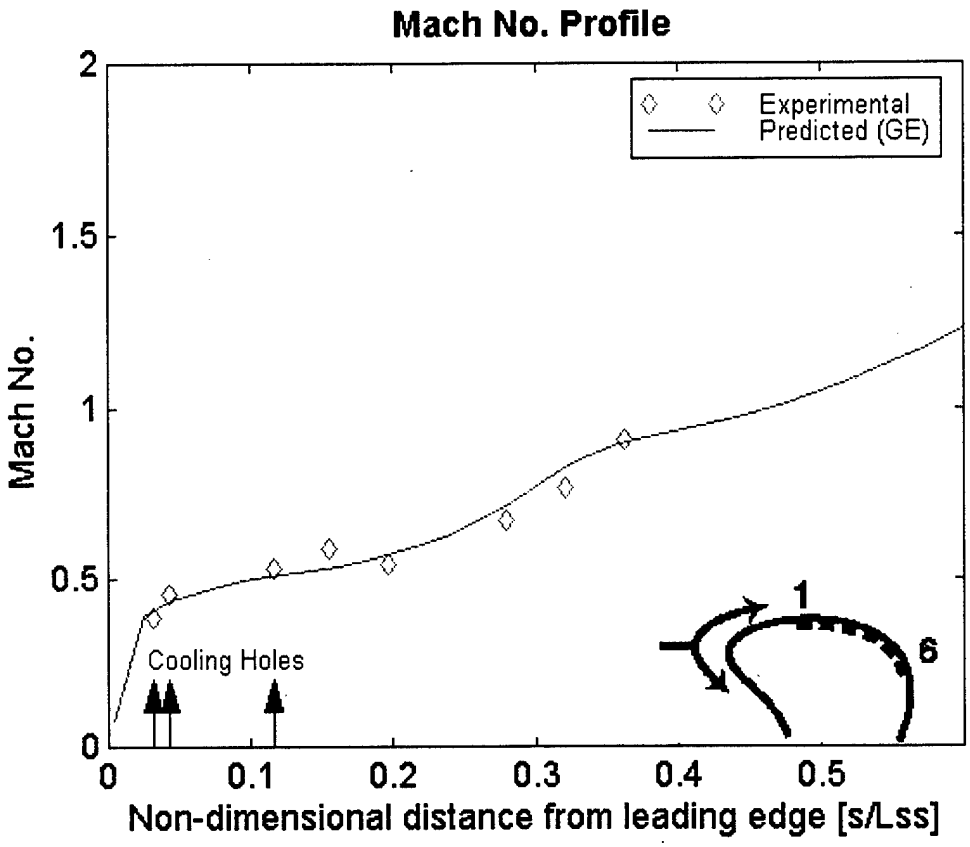

Figure 15: Mach Number Distribution Along Blade

Chapter 5: General Analysis

This study was performed in order to better understand the heat transfer taking place at the surface of turbine blades. An overview of the analysis used on the experimental data will be covered in this section. The dominant mode of heat transfer into the blade is convection, and the most important pieces of information are the steady heat transfer coefficient and the film cooling effectiveness. In low speed flows, convection heat transfer is characterized by the equation,

$$q = h \cdot (T_\infty - T_w) \tag{8}$$

where
T_∞ = the freestream total temperature in °C
T_w = the wall temperature in °C
h = heat transfer coefficient in W/(m·°C)
q = local heat flux in W/m

5.1 Uncooled Analysis

For high speed flows, such as those in turbines, the driving force of heat transfer is the recovery temperature and Equation (8) is rewritten as,

$$q = h \cdot (T_r - T_w) \tag{9}$$

where T_r is the recovery temperature. The recovery temperature can be calculated from the freestream total temperature using the equation,

$$T_r = T_\infty - (1 - r_c) \cdot \frac{u_\infty^2}{2 \cdot C_p} \tag{10}$$

where
u_∞ = the freestream velocity in m/s
C_p = the specific heat of the air in J/(kg·K)
r_c = the recovery factor

The recovery factor for laminar and turbulent flows is usually considered to be $Pr^{1/2}$ and $Pr^{1/3}$, respectively [Kays and Crawford, 1993]. The difference between the total freestream temperature and the recovery temperature is,

$$T_{o,\infty} - T_r = (1 - r_c) \cdot \frac{u_\infty^2}{2 \cdot C_p} \quad . \tag{11}$$

In all of the experiments in this work, the time histories of both the local heat flux and the wall temperature are known for the duration of the run, as can be seen in Figure 16. The dashed lines in the figure enclose the data which were used in the uncooled analysis. Approximately twenty seconds worth of data sampled at 100 Hz, about 2000 data points, were used in the analysis. The only unknowns in Equation (9) are the heat transfer coefficient, h, and the recovery temperature, T_r. The trace labeled T_r in the figure is the time history of the recovery temperature calculated from the measured freestream total temperature. The time history of the recovery temperature at each gauge location was generated using $T_{o,\infty}$ - T_r and Equation (10). Equation (9) can be rewritten using equations (10) and (11) to give,

$$q = h \cdot \left| \left(T_{o,\infty} - (T_{o,\infty} - T_r) \right) - T_w \right| \tag{12}$$

or,

$$q = h \cdot \left(T_{o,\infty} - T_w \right) - h \cdot (T_{o,\infty} - T_r) \tag{13}$$

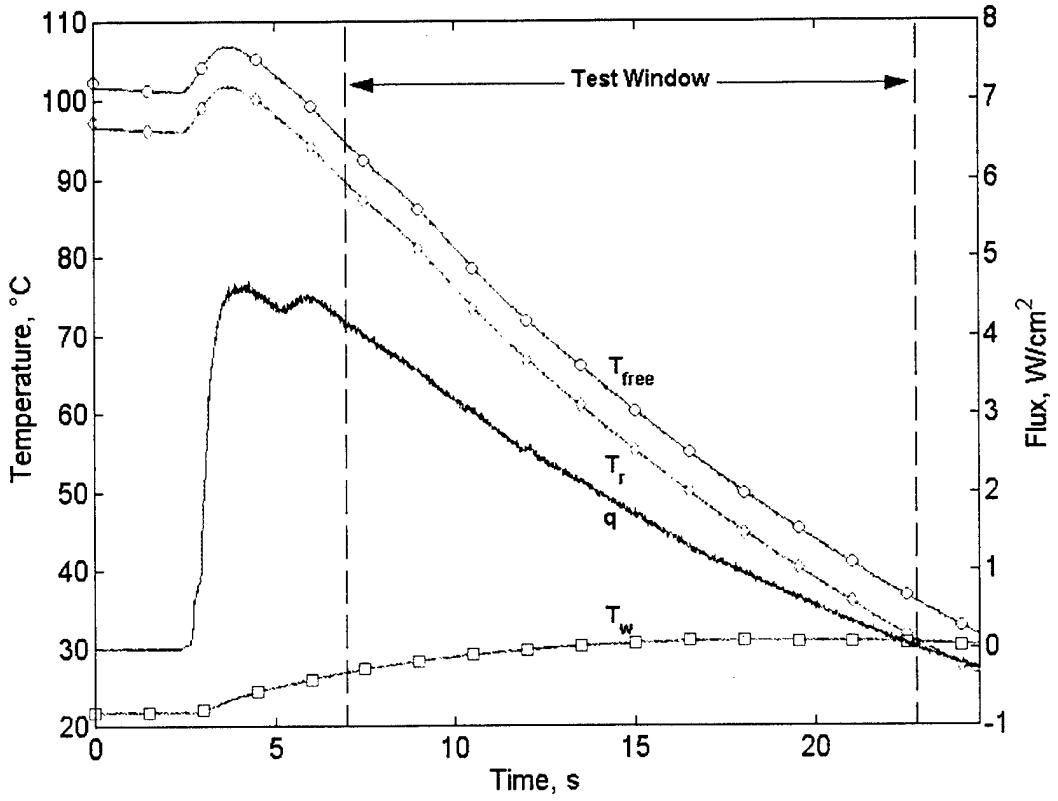

Figure 16: Sample Time History of an Uncooled Run

When the data from the time history of an uncooled run such as that shown in Figure 16 is plotted according to Equation (13), the result is a very linear curve in which the local heat flux is linearly dependent upon the difference between the freestream total temperature and the local wall temperature. A linear fit can be made through the data such that the slope of the line is the steady heat transfer coefficient and the intercept with the x-axis is the temperature difference, $T_{0,\infty} - T_r$. An example of the data plotted in this manner can be seen in Figure 17.

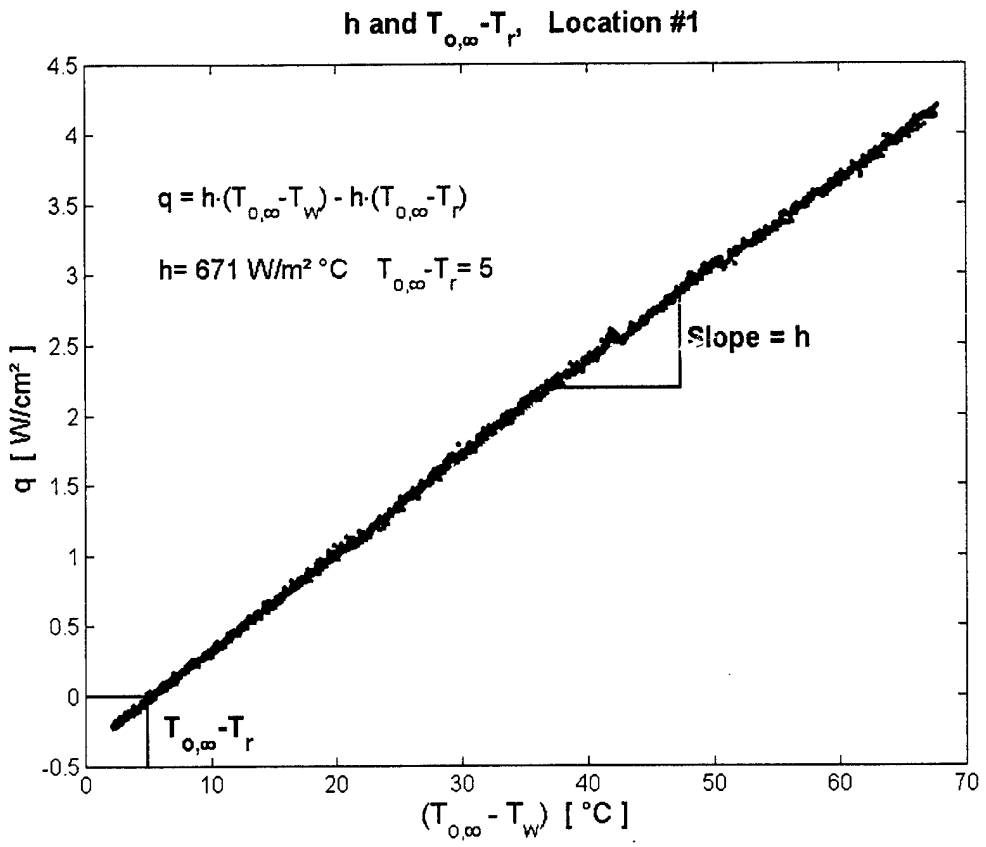

Figure 17: Data Analysis of an Uncooled Run

If the recovery temperature is known, the heat transfer coefficient can then be plotted as a function of time by using Equation (9). The time history of the recovery temperature is calculated by first assuming that the $T_{o,\infty}$ - T_r values determined in the analysis are constant over the run, and then by subtracting these values from the freestream total temperature. The assumption that the $T_{o,\infty}$ - T_r at every location is a constant over the run is supported by static pressure measurements which show that the Mach number distribution along the blade, and thus the flow field, remain constant throughout the run. Figure 18 is a typical plot of the time history of the heat transfer coefficient for uncooled runs. It can be seen that the heat transfer coefficient is constant over the course of the run and that the average value coincides with the value calculated from the linear fit. The magnitude of the oscillations about the mean value increases as

the run time progresses. This increase in oscillation is due to increased uncertainty as the flux approaches zero and is caused by the decrease in difference between the recovery and blade temperatures; effectively, the analysis is dividing a large number by a relatively small number.

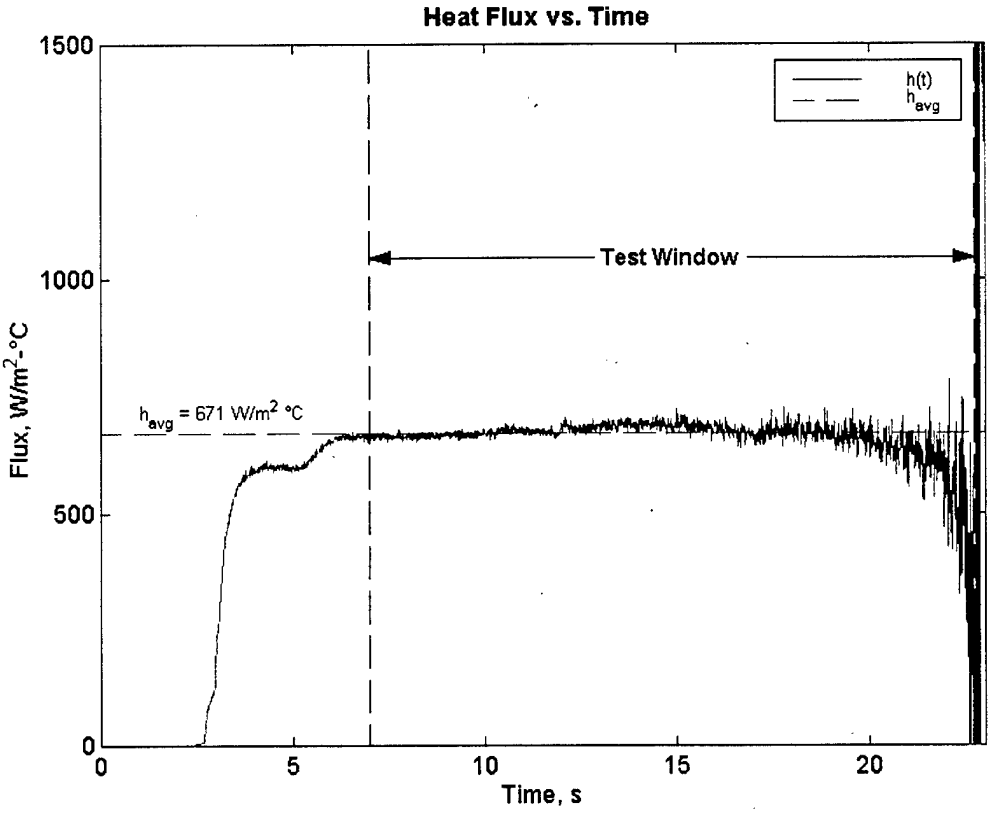

Figure 18: Time History of Heat Transfer Coefficient (uncooled)

As a consistency check of the analysis used on the uncooled data, the recovery and wall temperatures are plotted along with the local heat flux over the run. It should be noted that the local heat flux at this position approaches zero when the recovery and wall temperatures converge. Equation (9) shows that this is to be expected, so Figure 19 provides support for the values of h and $T_{0,\infty}$ - T_r found using this analysis.

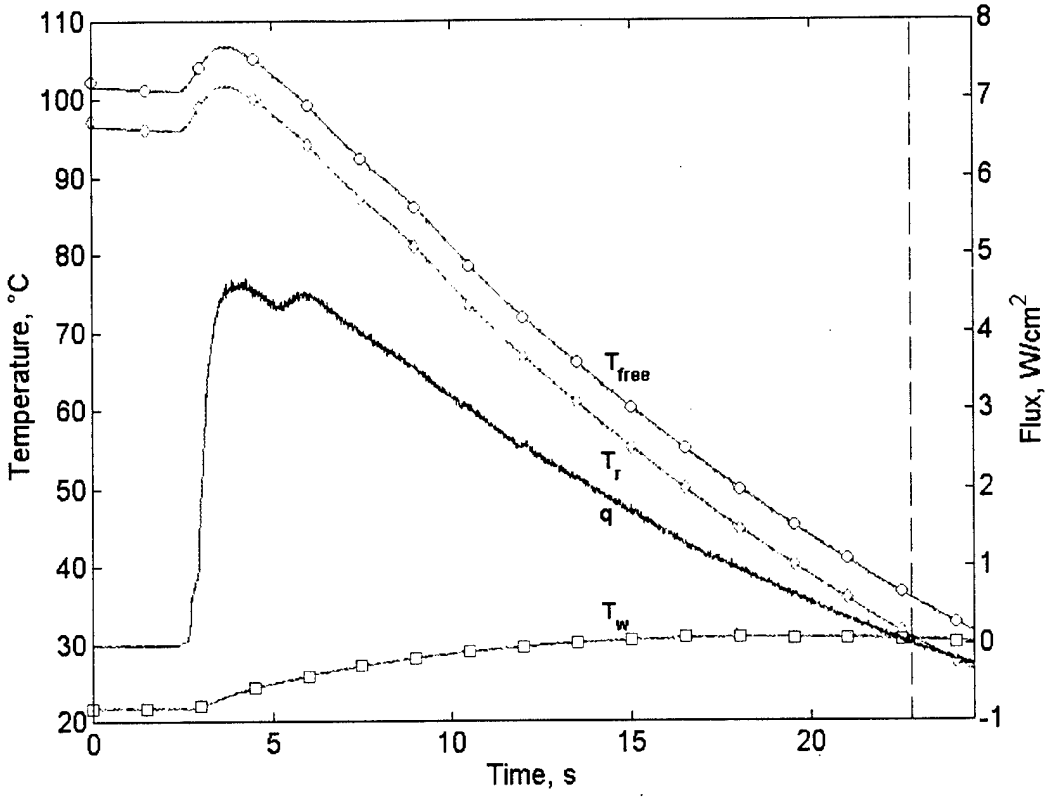

Figure 19: Consistency Check of Uncooled Analysis

5.2 Cold Coolant Analysis

Equation (9) is useful for cases where film cooling is not employed, but if fluid is injected into the boundary layer then the driving force of the heat transfer is dependent upon both the freestream and the injected fluid. For high speed flows with film injection equation (9) can be written as,

$$q = h \cdot (T_{aw} - T_w) \tag{14}$$

where T_{aw} is the driving force of the heat transfer. For high speed flows with no fluid injection, T_{aw} is equivalent to T_r. With coolant injection, however, the adiabatic wall temperature will lie in between the freestream and coolant temperatures(T_c); the

magnitude of T_{aw} depends upon the relative magnitudes of T_∞ and T_c as well as flow characteristics such as the blowing and density ratios.

T_{aw} is usually non-dimensionalized using a coolant characteristic called the film effectiveness, η, which is given in the equation (15),

$$\eta = \frac{T_{aw} - T_r}{T_c - T_r} \tag{15}$$

Solving for T_{aw} in equation (15) and substituting it into equation (14) yields,

$$q = h \cdot [(T_r - T_w) - \eta(T_r - T_c)] \tag{16}$$

which can be rearranged to give,

$$\frac{q}{(T_r - T_c)} = h \cdot \left[\frac{(T_r - T_w)}{(T_r - T_c)}\right] - h \cdot \eta \tag{17}$$

The temperatures of the wall, coolant, and freestream as well as the local heat flux into the turbine blade were all recorded for approximately 20 seconds during each run. The data recorded during a typical run with film cooling can be seen in Figure 20. The vertical dashed lines in Figure 20 indicate the portion of the data which was used in the analysis. It should also be noted that there is only one coolant temperature shown although there are three rows of coolant holes on the suction side of the blade. The coolant temperature time history shown is a mass average of the three rows of coolant jets. With these variables and the freestream velocity known, the recovery temperature can be calculated. The only unknowns in Equation (16), then, are the steady heat transfer coefficient and the film cooling effectiveness.

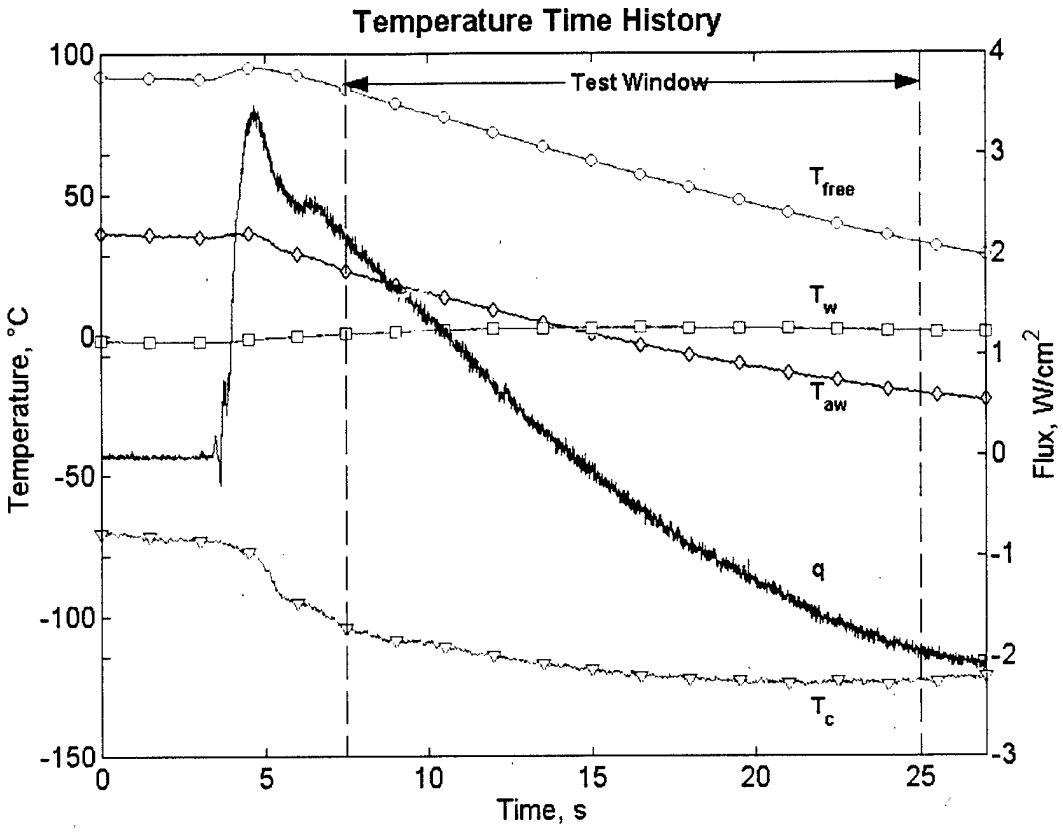

Figure 20: Sample Time History of a Film-cooled Run

If it is assumed that the heat transfer coefficient has only a weak dependence on temperature, then Equation (16) can be plotted such that the local heat flux divided by the recovery to coolant temperature difference (T_r - T_c) should be a linear function of a temperature difference ratio([T_r - T_w]/[T_r - T_c]). The slope of this linear curve is the steady heat transfer coefficient with film cooling and the x-axis intercept is the film cooling effectiveness. The mass averaged coolant temperature as well as the local wall temperature and heat flux are measured directly; the $T_{o,\infty}$ - T_r values calculated in the uncooled experiments were used in this analysis.

If the time history data from Figure 20 are plotted according to Equation (16), the result should be a straight line with the heat transfer coefficient equal to the slope and the film cooling effectiveness equal to the x-axis intercept. An example of the data plotted in

this manner is shown in Figure 21. It can be seen that the data is indeed linear which supports the assumption that the heat transfer coefficient has very little dependence on temperature over the range of temperatures used in this study. If the heat transfer coefficient had a strong dependence upon temperature then some trend other than linear should have been found.

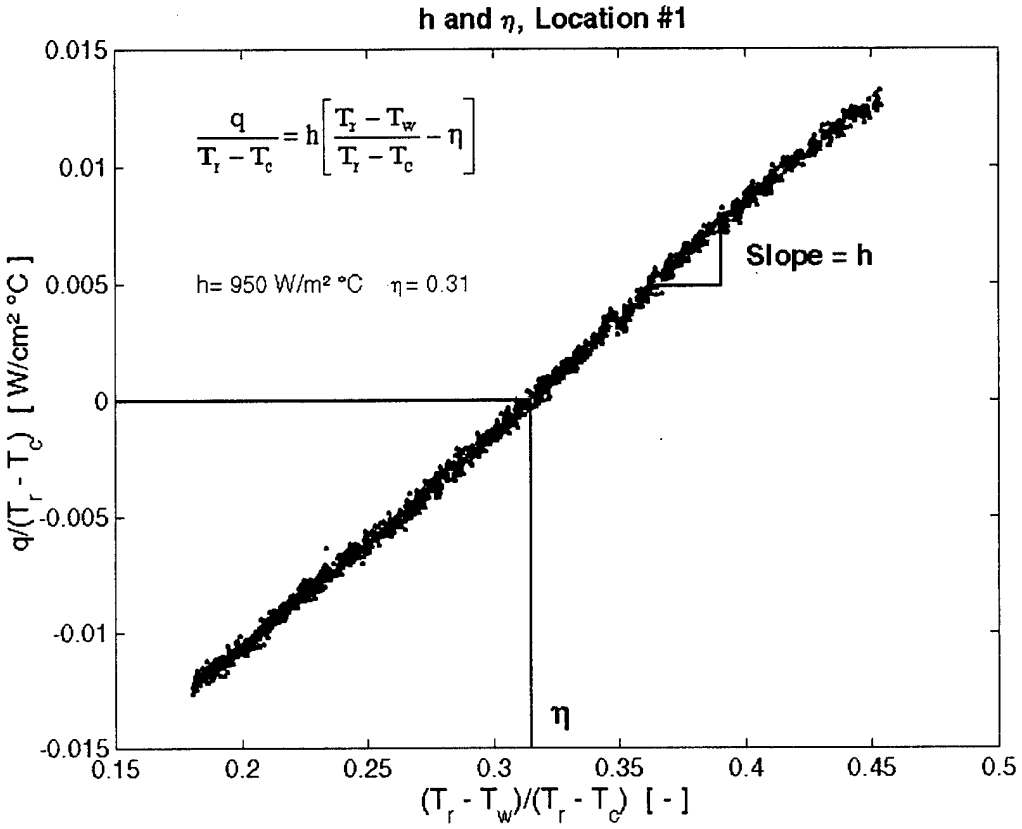

Figure 21: Film-cooled Data Analysis (cold coolant)

After determining values for the heat transfer coefficient and the film effectiveness, the adiabatic wall temperature for the film-cooled case can be determined and used to generate a time history of the heat transfer coefficient. This generated time history can be seen in Figure 22. The magnitude of the oscillations in heat transfer coefficient about the mean increase as the adiabatic wall temperature and the local wall

temperature converge. A comparison of the time when this convergence occurs on Figure 20 with the increase in oscillations on Figure 22 will show this relationship.

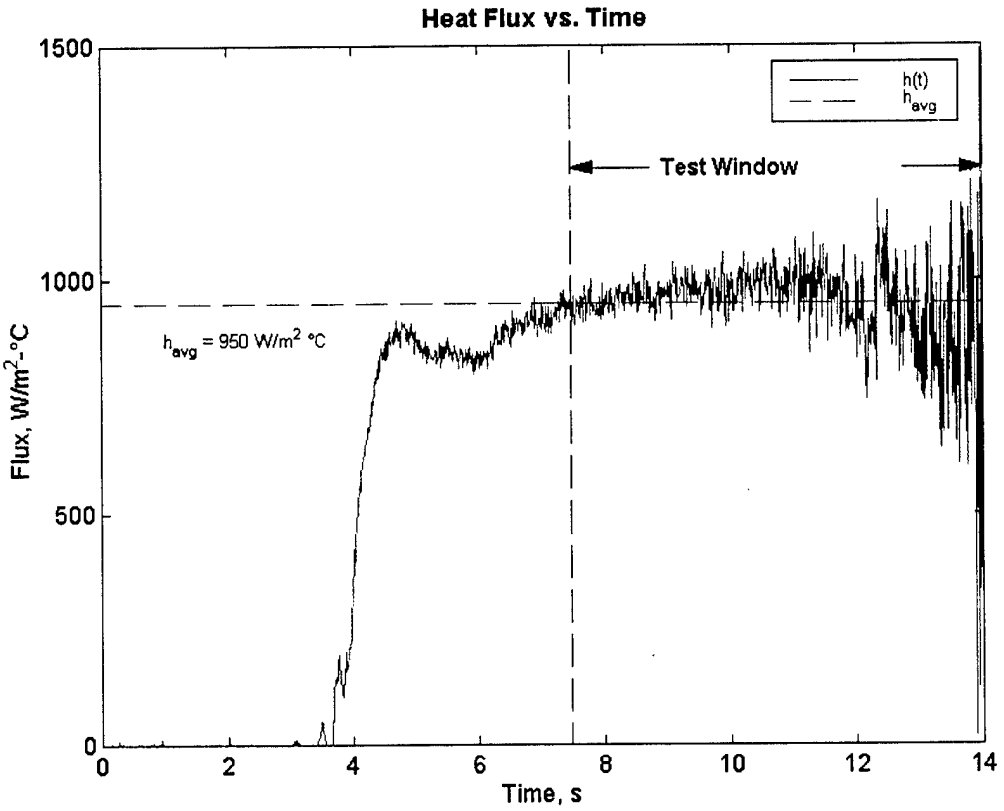

Figure 22: Heat Transfer Coefficient vs. Time (cold coolant)

Just as in the uncooled case, the heat transfer coefficient rises quickly from zero as flow enters the test section and then levels off at the value of the average heat transfer coefficient calculated in the cooled analysis earlier. The steady heat transfer coefficient with film cooling is a constant, like the uncooled case. This means that over the temperature ranges used in this study, the steady heat transfer coefficient with and without film cooling have a weak dependence upon temperature.

Chapter 6: Steady Heat Transfer Experiments

6.1 Uncooled Heat Transfer Experiments

6.1.1 Objectives

Steady heat transfer information about the 2-D turbine inlet rotor blade used in this study is important for understanding how blades like this may perform under actual engine conditions. The unsteady phenomena in the engine environment(shocks, wakes, etc.) cause variations in the mean heat transfer into the blade, but it may be that the mean heat transfer rate is what is of most importance to thermal designers of turbine blades [reference Oxford, 1995 & 1997]. The emphasis of this study is on the effects of film cooling on the steady heat transfer into the turbine blade, but as a baseline, the steady heat transfer coefficient and the recovery temperature on a blade without film cooling need to be determined.

6.1.2 Discussion

The data from the six uncooled runs were analyzed in the manner described in the uncooled analysis section of Chapter 5, and the results along the blade for the steady heat transfer coefficients without film cooling are displayed in Figure 26. The picture in the bottom right-hand corner of the figure shows the relative locations of the six HFM gauges on the suction side of the blade. The gauge locations have been non-dimensionalized using the suction side length. The average value of all locations, around 700 $W/m^2 \cdot °C$, is consistent with results reported in research done by other institutions given the flow conditions of the wind tunnel used in this work[reference appendix and sources].

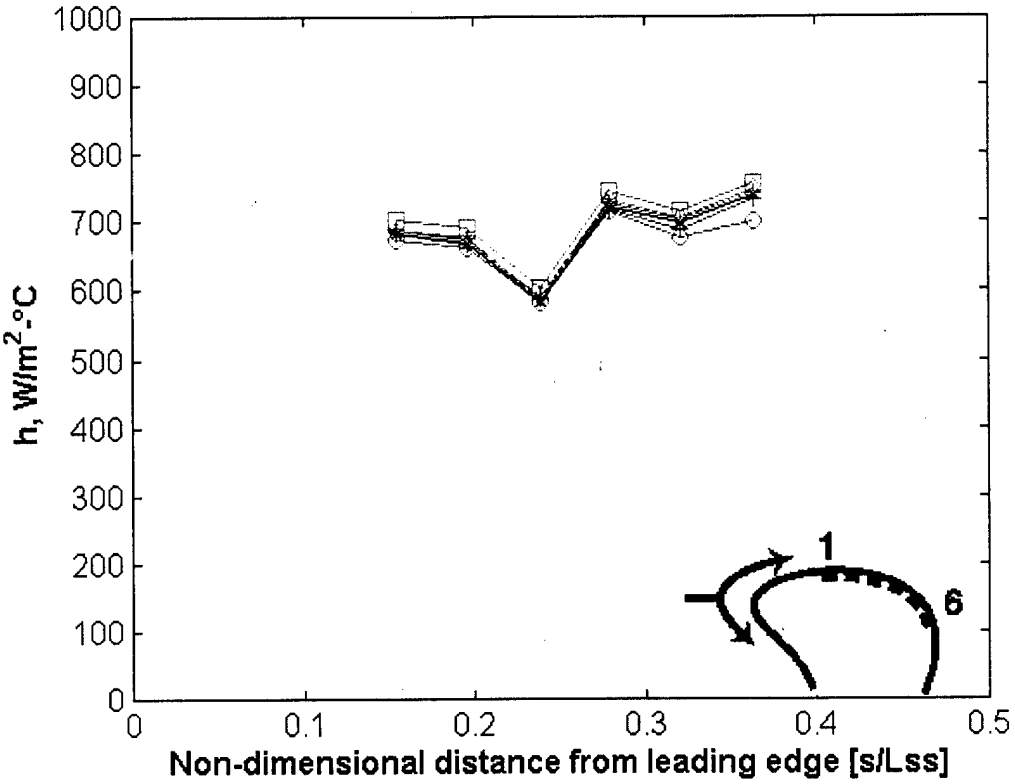

Figure 23: Uncooled Heat Transfer Coefficients Along Blade

The trend in the data from gauge location #1 back to gauge location #6 is unexpected, however. The suction side of the blade is similar to a flat plate with a pressure gradient. The heat transfer coefficient for a flat plate with no pressure gradient decreases with the distance from the leading edge. Therefore, it is expected that the suction side heat transfer coefficient should decrease as the non-dimensional length increases, but this is not the case in Figure 26. Initially, there is a decrease in heat transfer coefficient across the first three locations, but then there is a rise in heat transfer coefficient over the last set of gauges. There are many possible causes of this trend: non-two dimensional flow, disturbance caused by the coolant holes, the strong pressure gradient, or transition. Researchers at the Swiss Federal Institute noticed similar trends in the heat transfer coefficient on a turbine rotor blade without film cooling[Drost et al.,

1998]. By tripping the boundary layer, these researchers were able to get the expected decreasing trend in heat transfer coefficient. Time constraints prevented the boundary layer tripping technique from being performed before the conclusion of this study. However, the emphasis in this study was in finding the average level of the heat transfer coefficient under steady conditions to provide a basis for unsteady investigations, and this is not affected by the observed trends.

The value of $T_{o,\infty} - T_r$ calculated from experimental data can be plotted versus a predicted value based upon a correlation for the recovery factor in Equation (11) and knowledge of the freestream velocity. If it is assumed that the flow field is turbulent, the recovery factor can be approximated with $Pr^{1/3}$ [Kays and Crawford, 1990]. Knowing the Mach number distribution along the blade and using the approximated recovery factor, a prediction of the $T_{o,\infty} - T_r$ profile can be made. Figure 27 shows the experimental $T_{o,\infty} - T_r$ profile plotted along with the predicted value.

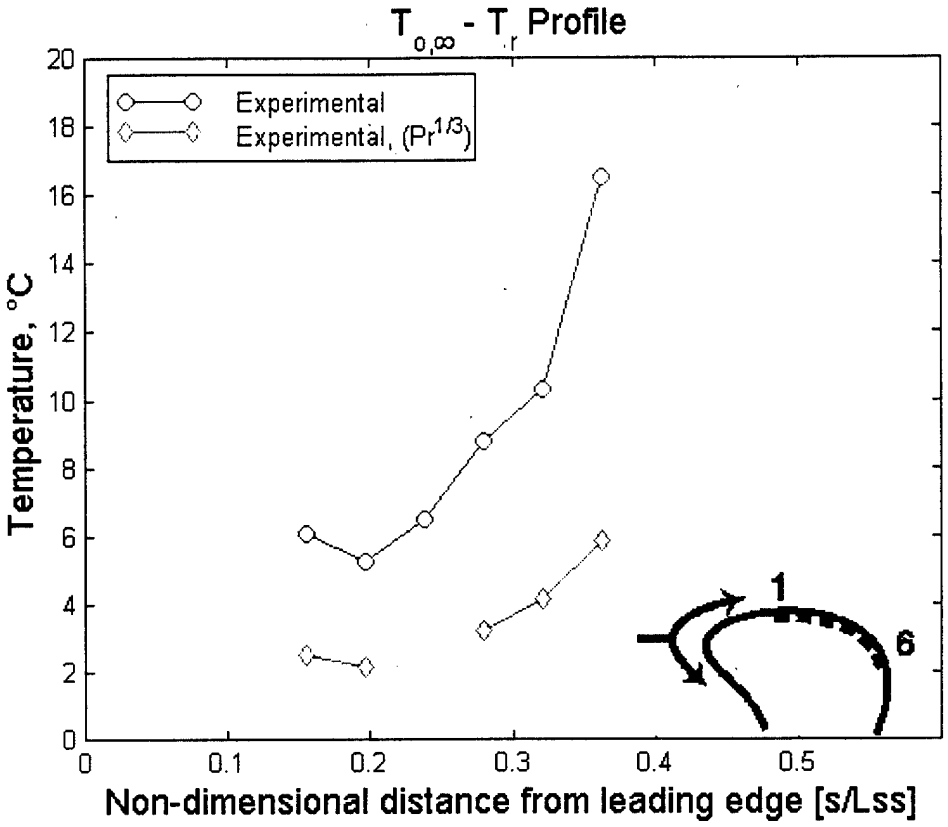

Figure 24: Comparison of Experimental and Predicted $T_{o,\infty}$ - T_r

This is a difficult measurement to make due to the uncertainties in temperature measurements, so some degree of imprecision is expected. The $T_{o,\infty}$ - T_r values calculated using experimental data in the uncooled analysis are smaller than the predicted values at all locations. However, the general trend is the same and the experimental and predicted values are of the same order of magnitude. This is an important point, because the two methods of determining $T_{o,\infty}$ - T_r are not linked. The experimental value is solely a function of the temperature and heat flux measurements made, while the predicted value depends on pressure measurements and the approximated recovery factor, $r_c = Pr^{1/3}$. This analysis is important because it provides a method of determining the recovery factor on turbine blades. The experimental values for $T_{o,\infty}$ - T_r at each gauge location were used to calculate the difference between the freestream and recovery temperatures

for all data calculations in the cold coolant runs. The effect of using the experimental values, as opposed to the predictions, on the steady heat transfer coefficient and film cooling effectiveness will be examined later in section 6.3.

6.2 Cold Coolant Heat Transfer Experiments

6.2.1 Objectives

Information about steady heat transfer with film cooling on the 2-D turbine inlet rotor blade used in this work is important in the design of future blades. Knowing the steady heat transfer coefficient and the recovery temperature on a blade without film cooling, a comparison can now be made to a blade with film cooling. The cold coolant heat transfer experiments were performed in order to investigate the heat transfer coefficient and the adiabatic film cooling effectiveness in order to determine the effect film cooling has on the turbine rotor blade used in this work.

6.2.2 Discussion

Data from all six gauges were gathered over six runs with film cooling. The dashed lines in Figure 20 represent the set of data that was actually used in the data analysis. Approximately twenty seconds of data were analyzed for each run with film cooling. Since the data was recorded at a sampling frequency of 100Hz, there are approximately 2000 data points gathered for each run. The coolant temperature shown is a mass averaged quantity determined from the temperatures and mass flows of the three rows of coolant holes whose injectants fold over onto the suction side. Figure 20 illustrates the transient nature of the experiments in the blow down wind tunnel.

The data from the six runs with a cold coolant injected as a film cooling layer were all analyzed in this manner. The results for the steady heat transfer coefficient along the blade with film cooling can be seen in Figure 28. The gauge locations are again plotted using the length of the suction side of the blade to non-dimensionalize the distance measured from the stagnation point to each gauge location. The three arrows in the bottom left of the figure represent the locations of the coolant hole on the suction side of the blade. Earlier, in Figure 14 a shadowgraph picture of the coolant flow was shown. This photograph indicates that only these three rows of coolant holes cover the suction side of the blade.

The average value of the film-cooled heat transfer coefficient, around 800 $W/m^2 \cdot °C$, is of the same order of magnitude as other researchers have found for cascade turbine blades with film cooling given the flow conditions of our wind tunnel and the geometry of our test section. A rise in heat transfer coefficient can be seen when the uncooled heat transfer distribution is compared to the film-cooled distribution. This rise in heat transfer coefficient is expected due to the increase in the level of turbulence caused by the injection of a cooling fluid into the boundary layer. However, the injected coolant also lowers the adiabatic wall temperature by an average of about 50°C. This decrease in the adiabatic wall temperature more than compensates for the rise in heat transfer coefficient, so the overall local heat flux into the blade is decreased by the injection of a cold fluid into the boundary layer.

The heat transfer coefficient distribution with film cooling displays trends similar to those found without film cooling. With film cooling, however, the initial decrease is more emphasized. It is suspicious that the injection of coolant into the boundary layer

has no effect on the location of the possible transition from laminar to turbulent flow. There is a lot of fluid being injected, and this disturbance should have caused any transition to occur earlier than in the uncooled case. The observed trend could still be the result of disturbances in the flow caused by the coolant holes or non-uniform spreading of the coolant film over the gauges. As stated earlier, however, the trend does not prevent the goal of this work from being achieved.

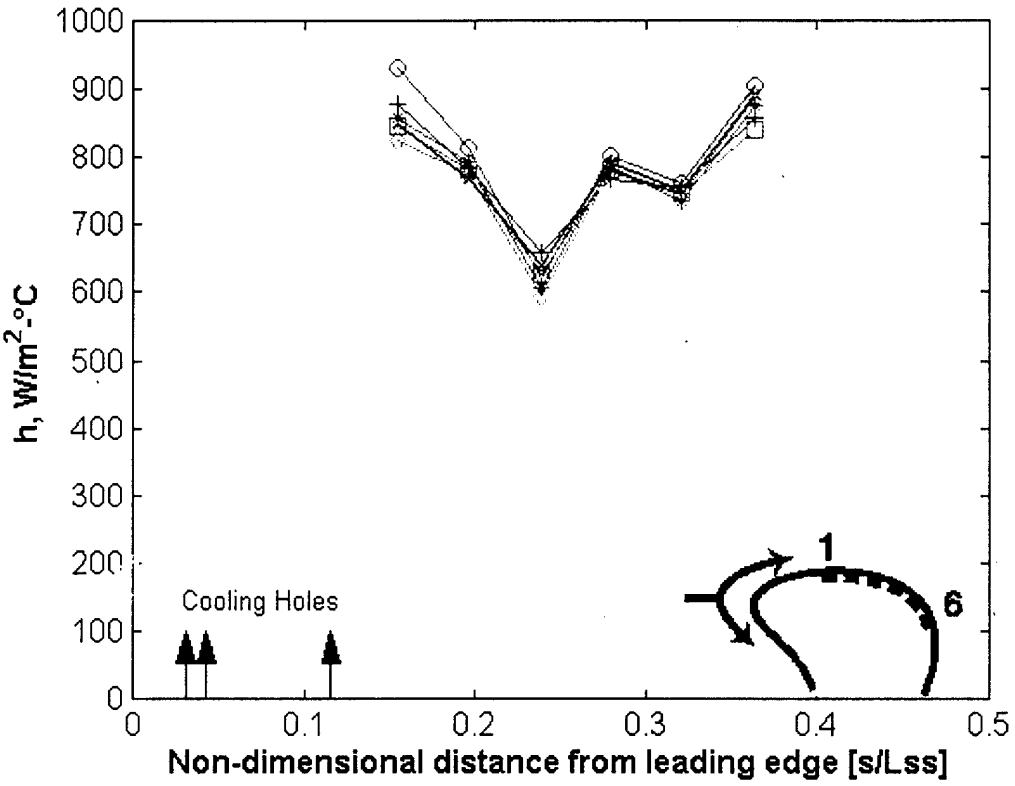

Figure 25: Cold Coolant Heat Transfer Coefficients Along Blade

Without further attempts to explain the observed trends in the heat transfer coefficient distribution along the blade, the rest of the film-cooled results will be presented. The results of the film cooling effectiveness distribution are displayed in Figure 29. The effectiveness distribution is plotted versus the same non-dimensionalized distance used earlier in Figures 23 - 25. The effectiveness of the film varies erratically up

and down from gauge to gauge as you move farther along the suction side of the blade. It is suspected that this variation has the same cause as the trends observed in heat transfer coefficient. The average value of the film cooling effectiveness is around 25%.

In the earlier section on the uncooled analysis it was mentioned that the recovery temperatures were calculated from the linear fit and not by using the correlation relating the Prandtl number to the recovery factor. The difference between the two methods was illustrated earlier in Figure 24. The effect the two methods of calculating recovery factor have on the film cooling effectiveness can also be seen in Figure 26. It is evident that using the experimental recovery factors does not have a major effect on the film cooling effectiveness.

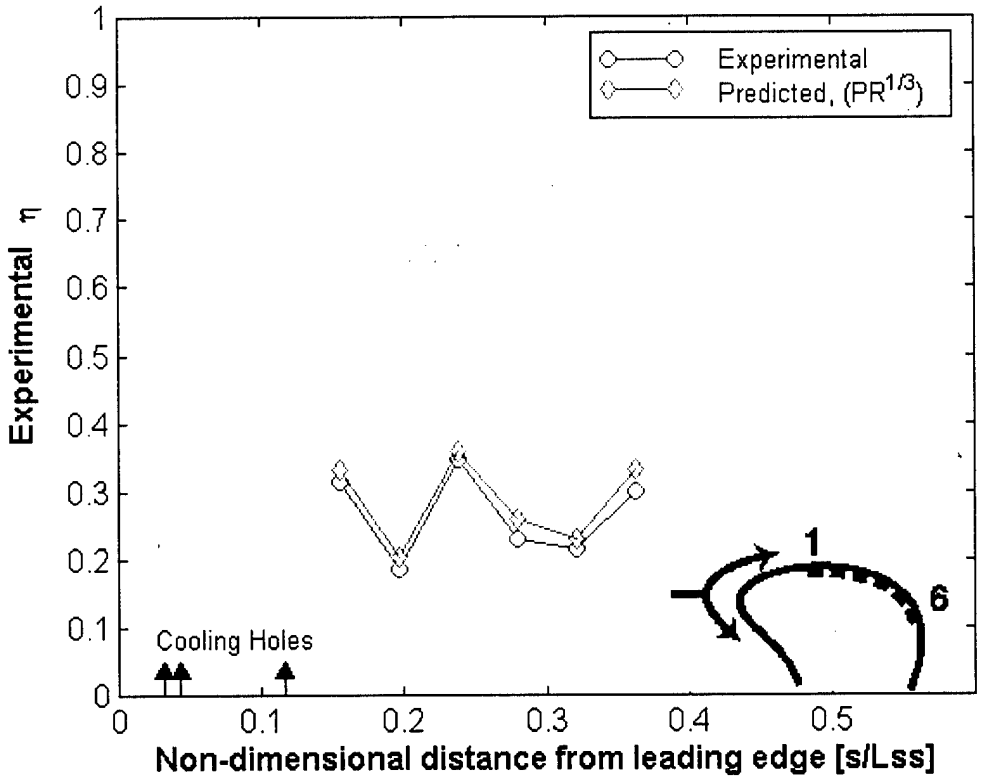

Figure 26: Effect of Experimental vs Predicted $T_{0,\infty}$ - T_r on eta

A comparison can be made of the steady heat transfer coefficient with and without film cooling present on the surface of the blade. Figure 27 shows the mean values from the six runs for both the uncooled and film-cooled cases. It is evident from this figure that presence of a film cooling layer increased the steady heat transfer coefficient along the blade.

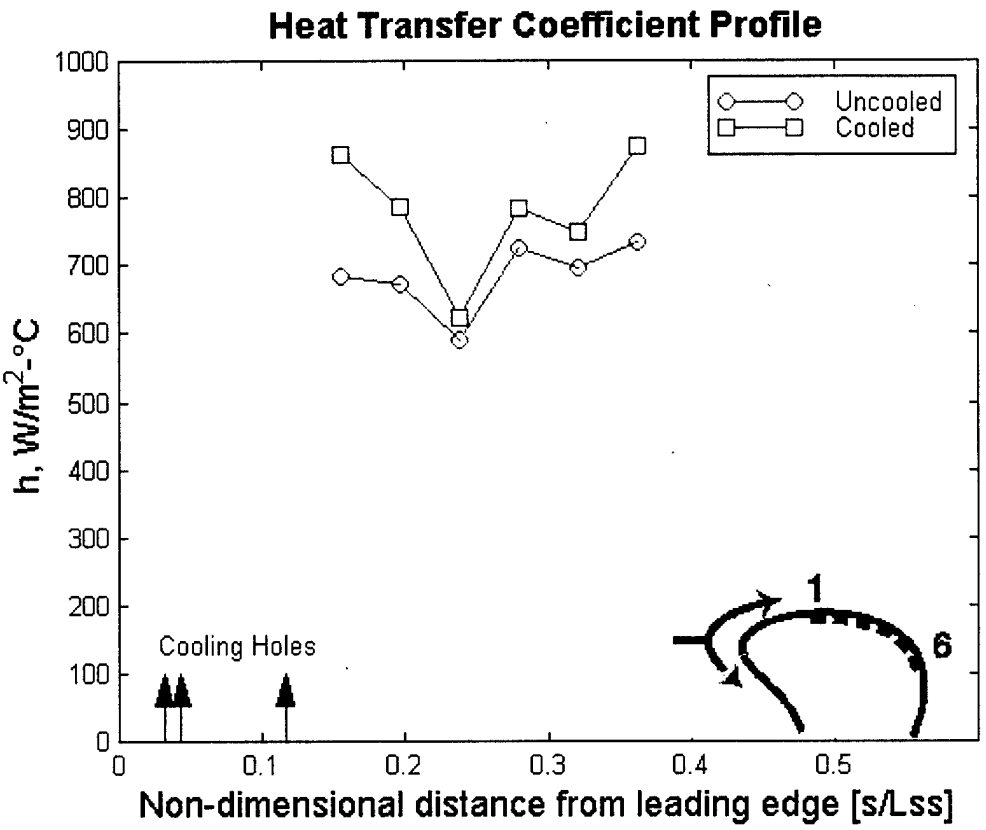

Figure 27: Comparison of Trends in h (uncooled, cold coolant)

The injection of the fluid disturbs the boundary layer and encourages mixing, both of which lead to the increase in heat transfer coefficient. Both the uncooled and the film-cooled results display the same trends; they are slightly more exaggerated in the film-cooled case, however. This figure shows that there is no change in the location of the transition region with the addition of film cooling. As stated earlier, this lack of response to the addition of film cooling suggests that the trends may not be the result of transition.

The actual values of the mean heat transfer coefficient of the six runs for both cases can be seen in Table 2. Also included in the table is the percent increase in heat transfer coefficient at each gauge location. The maximum increase of 26% occurs at the first gauge location which is approximately 9.4 hole diameters back from the last row of coolant holes. From the data in Table 2, it is evident that the percent increase in heat transfer coefficient from the uncooled case to the film-cooled case follows the same trend as seen in both cases separately.

Table 2: Comparison of Uncooled vs. Film-cooled Heat Transfer Coefficient

Gauge Location	Uncooled Heat Transfer Coefficient ($W/m^2 \cdot °C$)	Film-cooled Heat Transfer Coefficient ($W/m^2 \cdot °C$)	Percent Increase %
1	684	864	26
2	672	785	17
3	588	622	6
4	724	783	8
5	696	747	7
6	734	875	19

Chapter 7: Conclusions and Future Work

The instrumented turbine rotor blade was placed into the Virginia Tech Transonic Wind Tunnel where testing was performed. The Mach and Reynolds numbers at the exit of the test section were set to 1.2 and $5x10^6$,respectively, in order to simulate real engine flow conditions. The freestream and coolant flows were maintained at a total temperature ratio of 2 ±0.4 and a total pressure ratio of 1.04. The freestream turbulence level was approximately 1%. Two different sets of experiments were run: 1) heated mainstream flow with no film cooling, 2) heated mainstream flow with cold coolant.

Comparing the results of these two experiments showed that there was a decrease of heat transfer into the blades from the experiments without film cooling to those with film cooling, even though there was an increase in the steady heat transfer coefficient. The reason for the decrease in heat flux levels was the decrease in the adiabatic wall temperature, the driving force of the heat transfer, brought on by the injection of a cold coolant into the boundary layer. The average value of the heat transfer coefficient increased from 700 W/(m^2·°C) without cooling to 850 W/(m^2·°C) with film cooling. The average film cooling effectiveness along the blade was found to be 25%.

With the addition of film cooling, then, it can be concluded that the heat transfer coefficient increases approximately 21% over the section of the suction side of the rotor blade investigated in this work. From the uncooled runs, a difference was seen between the recovery temperature calculated using the uncooled analysis and the recovery temperature calculated using the correlation, $r_c = Pr^{1/3}$. This difference, approximately

6°C, is not significant in the calculation of the film cooling effectiveness because it is based upon temperature differences on the order of 80°C.

The results from both experiments displayed an unexpected trend in the heat transfer coefficient measured along the blade. In all cases, there is an initial decrease in heat transfer coefficient followed by a sudden increase almost back up to the starting level. This falling-rising trend in the heat transfer coefficient could be the result of either three-dimensionality in the flow-field (end wall effects, spanwise variations, etc.) or onset of the transition from a laminar to a turbulent boundary layer. The specific cause of the trends was not investigated in this study.

This work only investigated the steady heat transfer into a two-dimensional turbine inlet rotor blade. In the future, the cause of the trends in the steady heat transfer coefficient should be investigated. Oil drop visualizations could be performed along the span of the blade to check for spanwise variations and the boundary layer could be tripped near the leading edge to prevent transition from occurring later on the surface of the blade. In addition, the effect of different turbulence levels and blowing parameters on the steady heat transfer should be determined. Once the issues around the steady heat transfer into the blade have been resolved, the effects of unsteady events such as passing shocks and wakes should be investigated.

References

Abuaf, N., Bunker, R., Lee, C.P., G.E. Aircraft Engines, 1995, "Heat Transfer and Film Cooling Effectiveness in a LInear Cascade, " 40th IGTI Conference, ASME 95-GT-3.

Drost, U., Bölcs, A., Swiss Federal Institute of Technology, 1998, "Investigation of Detailed Film Cooling Effectiveness and Heat Transfer Distributions on a Gas Turbine Airfoil," ASME 98-GT-20.

Ekkad, S.V., Hui Du, and Je-chin Han, Texas A& M University, 1995, "Local Heat Transfer Coefficient and Film Effectiveness Distributions on a Cylindrical Leading Edge Model Using a Transient Liquid Crystal Image Method," ASME 95-WA/HT-3.

Goldstein, R.J., "Measurements in Heat Transfer," Hemisphere Pub. Corp., 1976.

Guo, S.M., Lai, C.C., Jeong, J.H., Jones, T.V., and Oldfield, M.L.G., University of Oxford, 1997, "Use of Liquid Crystal Techniques to Measure Film Cooling Heat Transfer and Effectiveness," 90th Symposium of the Propulsion and Energetics Panel, AGARD 20-24.

Guo, S.M., Jones, T.V., University of Oxford, and Lock, G.D., University of Bath, 1996, "Gas Turbine Heat Transfer Measurements with Engine Simulated Film Cooling," 2nd European Conference on Turbomachinery Fluid Dynamics and Thermodynamics, Technological Institute, Section on Aeronautics.

Horton, F.G., Shultz, D.L., Forest, A.E., University of Oxford, 1985, "Heat Transfer Measurements with Film Cooling on a Turbine Balade Profile in Cascade," ASME 95-GT-117.

Kays, W.M., Crawford, M.E., "Convective Heat and Mass Transfer," McGraw-Hill Inc., pp 380-388, 1993.

Schwarz, S.G., Goldstein, R.J., Eckert, E.R.G., Tulane University/University of Minnesota, 1990, "The Influence of Curvature on Film Cooling Performance," 35th IGTI Conference, ASME 90-GT-10.